V+ 2 Technical Manual Series: SkinDose Module

December 2024

Renaissance Code Development, LLC
310 NW 5th St., Suite 203
Corvallis, Oregon 97330
(541) 286-4428
https://www.rcdsoftware.com

Preparer: David Hamby DN: cn=David Hamby, o=Renaissance Code Development, ou=Operations Manager, email=david.hamby@rcdsoftware.com, c=US Date: 2025.03.27 15:02:32 -07'00'

Reviewer: Roland R. Benke DN: cn=Roland R. Benke, o=Renaissance Code Development, ou=General Manager, email=roland.benke@rcdsoftware.com, c=US Date: 2025.03.28 14:19:32 -05'00'

Approver: Jeffrey Luitjens cn=Jeffrey Luitjens, o=Renaissance Code Development, ou=Director - Software Division, email=jeff.luitjens@rcdsoftware.com, c=US 2025.03.28 15:42:49 -07'00'

ABSTRACT

VARSKIN+ (V+) is a U.S. Nuclear Regulatory Commission (NRC) computer code used by staff members and NRC licensees to calculate occupational dose to the skin resulting from exposure to radiation emitted from hot particles or other contamination on or near the skin. These assessments are required by Title 10 of the *Code of Federal Regulations* (10 CFR) 20.1201(c), which states that the assigned Shallow Dose Equivalent (10 CFR 20.1003) is to the part of the body receiving the highest exposure over a contiguous 10 cm^2 of skin at a tissue depth of 0.007 centimeters (7 mg/cm^2), implying unit-density tissue.

The V+ SkinDose module, an algorithm to calculate skin dose from radioactive skin contamination, has been modified on several occasions. As in previous versions, predefined source configurations are available in SkinDose to allow simulations of point, disk, cylinder, sphere, slab, and syringe sources. Improvements to earlier versions included enhanced photon, electron, and alpha dosimetry models, as well as models to account for airgap and cover materials. SkinDose gives the user the option to have the code automatically include all decay products in dosimetry calculations or to allow the user to manually add progeny. Both ICRP 38, "Radionuclide Transformations – Energy and Intensity of Emissions" (1983), and ICRP 107, "Nuclear Decay Data for Dosimetry Calculations" (2008), nuclide libraries are available at the user's option and contain data on gamma rays, X rays, beta particles, alpha particles, internal conversion electrons, and Auger electrons. Although the user can choose any dose-averaging area, the default area for skin dose calculations is 10 square centimeters, to conform to the requirements in 10 CFR 20.1201(c). A variety of unit options are provided (including both British and International System (SI) units), and the source strength can be entered in units of total activity or distributed in units of activity per unit area. The photon model accounts for photon attenuation, charged particle buildup, and electron scatter at all depths in skin. The model allows for volumetric sources and clothing or airgaps between source and skin. The electron dosimetry model has a robust accounting for electron energy loss and particle scatter. Dose point kernels are Monte-Carlo based and results agree very well with Electron Gamma Shower (EGS) and Monte Carlo N Particle (MCNP) probabilistic simulations. The alpha dosimetry model assumes a more accurate tissue density of 1.1 g/cm^3 to fully describe energy loss as a function of track length.

Table of Contents

LIST OF FIGURES

LIST OF TABLES

ACKNOWLEDGMENTS

This report documents the work performed by Renaissance Code Development, LLC (RCD) for the U.S Nuclear Regulatory Commission (NRC) under previous contracts and the current Contract No. 31310022C0011. Staff at the Pacific Northwest National Laboratory authored initial versions of VARSKIN (US NRC 1987; US NRC 1989), with later versions amended at Colorado State University (US NRC 1992), the Center for Nuclear Waste Regulatory Analyses (US NRC 2006), Oregon State University (US NRC 2011; US NRC 2014; US NRC 2018), and Renaissance Code Development (US NRC 2020). RCD performed the activities described herein on behalf of the NRC Office of Nuclear Regulatory Research, Division of Systems Analysis. This report is a product of RCD and does not necessarily reflect the views or regulatory position of the NRC.

The authors are indebted to S. Bush-Goddard, B. Allen, R. Flora, V. Shaffer, J. Tomon, M. Saba, and S. Sherbini for their support during development and maintenance of many of the dosimetry models now appearing in SkinDose.

1.0 INTRODUCTION

The original VARSKIN computer code (US NRC 1987) was intended as a tool for the calculation of tissue dose at user-defined depths as the result of skin surface contamination. The contamination was assumed to be a point, or an infinitely thin disk source located directly on the skin surface. Soon after the release of VARSKIN, the industry encountered a “new” type of skin contaminant consisting of discrete microscopic radioactive fragments, called “hot particles”. These particles differ radically from uniform skin contamination in that they have a volume associated with them and many of the skin exposures result from particles on the outside of protective clothing. These assessments are required by Title 10 of the Code of Federal Regulations (10 CFR) 20.1201(c), which states that the assigned shallow dose equivalent (SDE; 10 CFR 20.1003) is to the part of the body receiving the highest exposure over a contiguous 10 cm^2 of skin at a tissue depth of 0.007 centimeters (7 mg/cm^2).

VARSKIN MOD2 (US NRC 1992) contained all the features of the original VARSKIN, with many significant additions. Features in MOD2 included the modeling of three-dimensional (3D) sources (cylinders, spheres, and slabs) that accounted for self-shielding, and modeling of materials placed between the source and skin (i.e., airgaps and covers) that could absorb electron energy and attenuate photons. VARSKIN MOD2 also used a correction for backscatter for one-dimensional and two-dimensional (2D) electron sources under limited conditions. Finally, the VARSKIN MOD2 package incorporated a user interface that greatly simplified data entry for calculating skin dose.

MOD2 contained a volume-averaging dose model that has been retained in subsequent VARSKIN coding. The volume-averaging model allows the user to calculate dose averaged over a volume of tissue defined by a cylinder with a diameter equal to that of the dose-averaging area and bounded at the top and bottom by two user-selected skin depths (Figure 1-1). This model is useful for calculations of dose that can be compared to the dose measured by a finite-volume instrument (e.g., a thermoluminescent dosimeter).

Additionally, VARSKIN MOD2 gave the user the ability to select a composite source term, thus allowing the calculation of total dose from a mixture of radionuclides instead of requiring the code to be executed separately for each constituent. This feature was upgraded in VARSKIN 3 (US NRC 2006), allowing the user to select up to twenty radionuclides in a single calculation. One drawback of removing this feature in VARSKIN 3 was that the user was forced to explicitly add radioactive progeny. Subsequent VARSKIN versions incorporate radioactivity progeny at the user’s discretion.

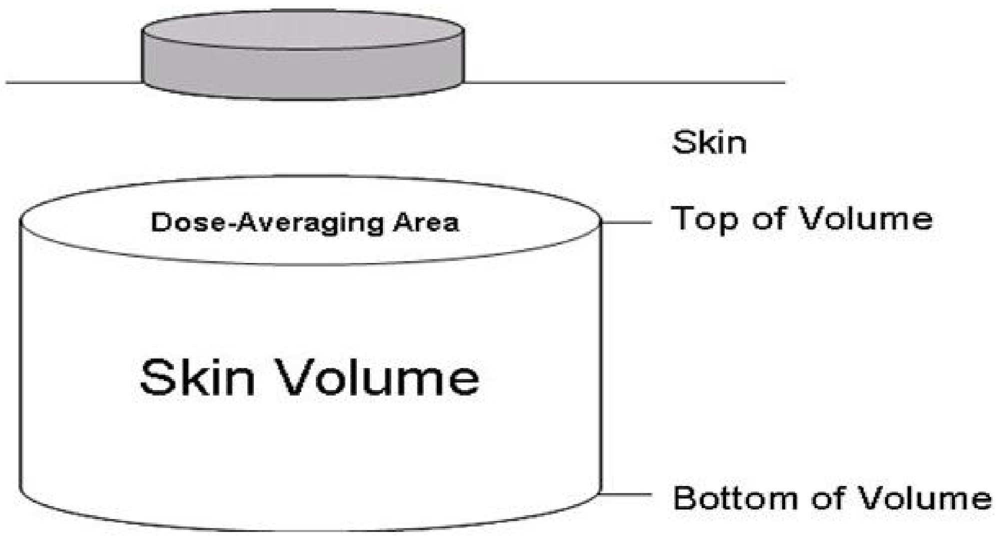

Figure 1-1. Depiction of Cylindrical Dose Averaging Volume (US NRC 1987)

Enhancements to VARSKIN 4 (US NRC 2011) focused on the photon dosimetry model. The photon model includes charged-particle buildup and subsequent transient equilibrium, along with photon attenuation, air and cover attenuation, and the option to model volumetric sources. The VARSKIN 5 (US NRC 2014) package updated electron dosimetry model to better account for charged-particle energy loss as the particle moves through the source, cover material, air, and tissue. VARSKIN 6 (US NRC 2018) further enhanced the physics models and the user interface. SkinDose, introduced in VARSKIN+ (US NRC 2021), employs a new user interface written in Java and updated Fortran for physics calculations based on Fortran 2018 fundamentals. Speed increases of 25x have been realized in various data-handling routines of the updated Fortran.

SkinDose calculates dose equivalent from photon, electron, and alpha radiation from more than 1,200 radionuclides that may be encountered in a variety of skin-contamination applications from laboratory use to medical and therapeutic applications. SkinDose can calculate the dose to 2D averaging areas from a minimum of 0.01 cm^2 to a maximum of 100 cm^2, and airgaps between source and skin of up to 20 cm. SkinDose calculates shallow dose to an infinitely thin disk at a depth of 7 mg/cm^2 in tissue for comparison to the NRC shallow dose limit of 0.5 gray (Gy) for both point and distributed sources. Other user-specified depths from zero to 2 cm are allowable. Users are cautioned that SkinDose is designed to calculate the dose to skin from skin contamination or sources close to the skin surface (within 20 cm). Using SkinDose to perform calculations that are beyond its intended application may result in erroneous dose estimates. SkinDose offers the option of dose calculations based on the decay data of International Commission on Radiological Protection (ICRP) 38, “Radionuclide Transformations – Energy and Intensity of Emission” (ICRP 1983), or ICRP 107, “Nuclear Decay Data for Dosimetric Calculations” (ICRP 2008).

2.0 SKIN DOSIMETRY MODEL

SkinDose (classic VARSKIN) uses robust electron (Mangini 2012; US NRC 2014; Mangini and Hamby 2016), photon (US NRC 2011), and alpha skin dosimetry models.

SkinDose calculates dose to an infinitely thin disk at depth in tissue for comparison to the NRC shallow dose limit of 0.5 Gray (Gy) for both point and distributed sources (10 CFR 1201(a)(2)(ii)). SkinDose can calculate the dose to averaging areas from a minimum of 0.01 cm^2 to a maximum of 100 cm^2. Users are cautioned that SkinDose is designed to calculate the dose to skin from skin contamination. Using SkinDose to perform calculations that are beyond the intended application of the code may result in erroneous dose estimates.

SkinDose offers the option of dose calculations based on the decay data published in ICRP 38 (1983) or ICRP 107 (2008). ICRP 38 offers 838 radionuclides in the main library, while ICRP 107 offers more than 1,200.

Dose calculations involving airgaps greater than 20 cm have not been tested and are, therefore, not allowed. It is likely that erroneous results would be obtained for large airgaps because the code will not account for multiple scattering events in air. These events may result in the dose being delivered to an area greater than that determined using SkinDose and can lead to inaccurate results. SkinDose is limited such that calculations for airgaps greater than 20 cm are not possible and a warning message is displayed.

SkinDose has not been tested extensively for dose-averaging areas other than 1 and 10 cm^2. However, because of the nature of the calculations performed by SkinDose, there is no reason to believe that doses to areas less than or greater than 10 cm^2 will result in errors. A limited study of dose results as a function of averaging disk area shows that the code appears to be stable and linear in this regard from 0.01 to 100 cm^2 (US NRC 2014).

2.1. Electron Dosimetry

As with SkinDose, dosimetry codes based on the dose-point kernel (DPK) method rely on the numerical integration of a point kernel over the source volume and dose region of interest. While this is computationally much faster than a Monte Carlo simulation, accuracy is often sacrificed with the point kernel simplification. In one way or another, all DPKs relate the dose at a given point to a radiation source at some other point in a homogeneous medium. The medium for which the DPK is defined is typically water, as this allows for direct comparison with tissue. If the medium is not water, various scaling techniques (discussed later in this section) can be used to quantify energy loss along the charged particle track and to simulate the scatter of particle energy.

2.1.1. Dose-Point Kernels

Dose rates in SkinDose are calculated through numerical integration methods where DPKs are integrated over the entire source volume and dose-averaging area. The point kernel is given by (Eq. [2.1]):

$$D_\beta(r)\left[\frac{Gy}{sec}\right] = \frac{1.6x10^{-10}\left[\frac{J\,\mathrm{g}}{MeV\,\mathrm{kg}}\right]\cdot A\left[\frac{dis}{sec}\right]\cdot Y\left[\frac{\beta}{dis}\right]\cdot \overline{E_\beta}\left[\frac{MeV}{\beta}\right]\cdot F_\beta(\xi)}{4\pi r^2\cdot \rho\left[\frac{g}{cm^3}\right]\cdot X_{90}[cm]} \tag{2.1}$$

where $F_\beta(\xi)$ represents a scaled absorbed dose distribution (Berger 1971; Mangini 2012). The parameter ξ represents the density scaled distance (includes distances in the source cover, clothing, and air) from the source point to the dose point, written as a ratio normalized to the X_{90} distance. The distance r is the physical distance between the source point and the dose point. The distance X_{90} is the distance in which 90 percent of the primary electron's kinetic energy is absorbed.

The ongoing development of Monte Carlo electron transport codes includes tabulation of increasingly accurate electron DPKs. The main advantage of Monte Carlo-based energy deposition kernels (EDK) is the ability to account for energy-loss straggling and provide more accurate results for ranges above 90 percent of the X_{90} distance. SkinDose calculates $F_\beta(\xi)$ using the Monte Carlo based EDKs ($I(r)$) described below, thereby replacing Spencer's (1955, 1959) moment-based energy dissipation distributions used in the VARSKIN software through V4.0.

The Monte Carlo transport code, Electron Gamma Shower (EGSnrc) (Ljungberg et al. 2012), was used to determine the radial energy distributions (or DPKs) and X_{90} values at electron energies of 0.01 MeV ≤ E ≤ 8 MeV (32 total energies). An isotropic monoenergetic point source was positioned at the center of concentric spherical shells of the respective media. For all simulations, the shell thickness was 5 percent of the continuous slowing down approximation (CSDA) electron range, as taken from the National Institute of Standards and Technology (NIST) "Stopping Power and Range Tables for Electrons" (ESTAR) and depicted in Figure

2-1. The last shell was at a radius 150 percent of the CSDA range to ensure complete absorption of the electron energy (excluding radiative losses). The maximum energy of 8 MeV covers all beta-particle endpoint energies published in ICRP 107 (2008). The minimum energy of 0.01 MeV is based on the 0.001 MeV lower limit of electron cross-section data available in the EGSnrc software. Additionally, the ESTAR CSDA range of a 0.01 MeV electron is 0.252 mg cm^{-2} and far less than 7 mg cm^{-2}.

The National Research Council of Canada updated the EGS software to create EGSnrc. The EGSnrc simulations were performed using the EDKnrc user code. The EDKnrc code can be used to calculate EDKs for photons or electrons (monoenergetic or polyenergetic) forced to interact at the center of a spherical geometry. The code can output EDKs in user-defined spherical shells. The number of particle histories was set to one million and transport parameters were set to default settings except that: (1) PEGS datasets are used with AE=AP=1 keV; (2) ECUT=PCUT=1 keV (where AE, AP, ECUT and PCUT represent the delta value in restricted stopping powers for electrons and photons); (3) Rayleigh scattering is turned on; and (4) bremsstrahlung cross sections are set to NIST standards.

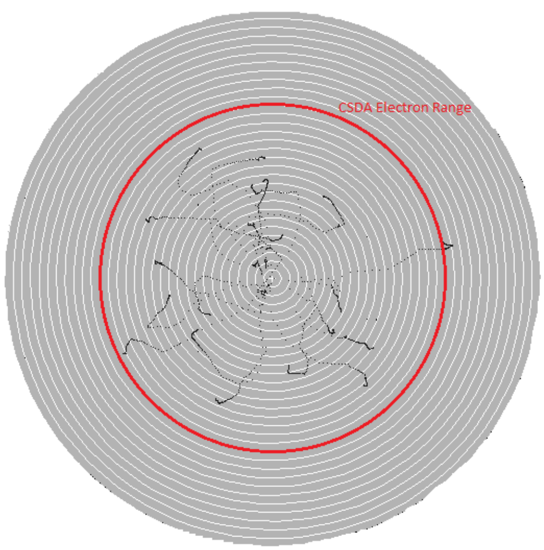

Figure 2-1. Schematic of EGSnrc Geometry for Determining Point-Source Radial DPKs

PEGSs datasets are the material cross section data used by EGSnrc. The parameters of AE and AP determine the lowest energy for which the cross-section values are defined for electrons and photons, respectively. Generally, when AE and AP are lowered (minimum of 1 keV), the accuracy of the calculation increases; however, the computation time increases as well (Kawrakow and Rogers 2000).

Electrons with energies below AE will not be transported and their energy is assumed to deposit locally. The same is true for photons (AP). The parameters ECUT and PCUT are related to AE and AP in that when an electron/photon energy falls below ECUT/PCUT, its energy is assumed to deposit locally. It is not possible to set ECUT and PCUT below AE and AP, respectively. The two parameters, ECUT and PCUT, represent the *Δ* value in restricted stopping powers.

Turning on the Rayleigh scattering parameter allows for the simulation of coherent scattering. Raleigh scattering for bremsstrahlung photons may become important below ~1 MeV for high-Z materials and below 100 - 200 keV in low-Z materials. The updated NIST database for nuclear bremsstrahlung is strongly recommended for electron energies below 1 - 2 MeV with negligible improvements over default Bethe-Heitler cross sections above ~ 50 MeV. Sampling from the NIST database is faster at low energies but slower at high energies (Kawrakow and Rogers 2000).

Once the EDKs were determined at CSDA range increments, the X_{90} values for each energy were determined and the kernels are tabulated with respect to ξ, the unitless ratio of electron range to the X_{90}. These kernels were then read into SadCalc.exe for use in the SADD (scaled absorbed dose distribution) subroutine and SPENS function. As stated previously, the main advantage of Monte Carlo-based EDKs over moment-based kernels is the ability to account for energy-loss straggling, thereby improving dose estimations with depth. This is easily seen by plotting $F(\xi,E_0)$ values determined using both moment-based (VARSKIN 4 and earlier) and Monte Carlo-based (VARSKIN 5 and later) methods (Figure 2-2 and Figure 2-3).

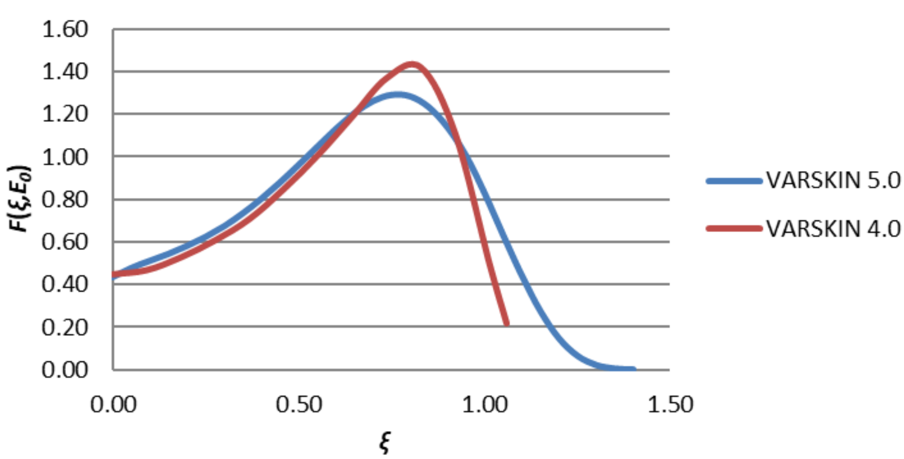

Figure 2-2. Scaled Absorbed Dose Distributions for 0.1 MeV Electrons in an Infinite Homogeneous Water Medium

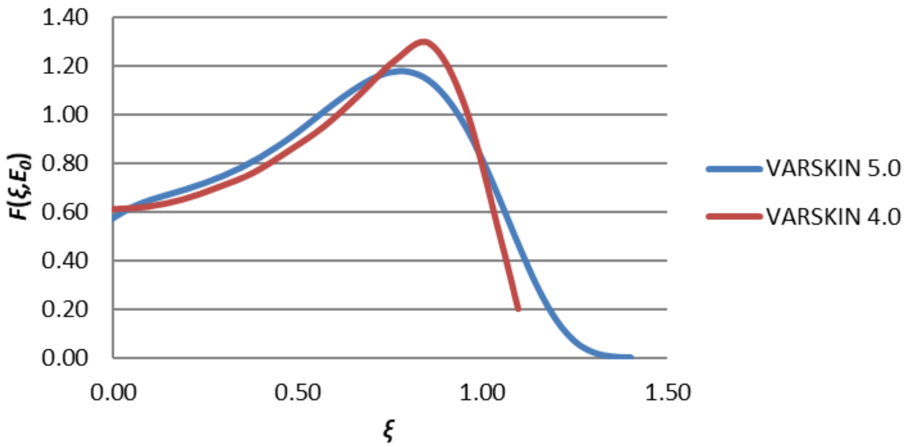

Figure 2-3. Scaled Absorbed Dose Distributions for 1.0 MeV Electrons in an Infinite Homogeneous Water Medium

2.1.2. Numerical Integration of Dose-Point Kernels

DPK codes rely on an accurate and fast numerical integration method to calculate dose from a volumetric source to a given dose area. A typical integration process divides the source into very small sub-volumes (source points). The dose-averaging area is divided into points at which the dose rate is to be calculated (dose points). The dose points (60 are used in SkinDose) are positioned along the radius of a dose-averaging disk at a specified dose depth (Figure 2-4). Since the source geometry (this discussion uses cylindrical) is symmetric about the dose-averaging area, dose points represent concentric isodose circles that describe the radial dose profile at a given depth in skin.

For each of the sixty dose points, a numerical integration is performed over the area of the cylindrical source at a given height in the source represented by eight elevations (z), eight radii (r'), and eight angular locations (θ). The dose rate at a dose point on an isodose circle of radius d' is evaluated using Eq. [2.2]

$$D(d') = S_v \int_0^{2\pi} \int_0^{R} \int_0^{Z} r'\, B(z, r', \theta)\; dz\; dr'\; d\theta \qquad [2.2]$$

where $B(z,r',\theta)$ is the dose per disintegration (rad nt^{-1}) from a source point with source-coordinates (cylindrical) of z, r', and θ; R and Z are the source radius and height; and S_v is the volumetric source strength (nt cm^{-3}). This procedure is repeated for each dose point beginning at the center of the irradiation area and extending to its edge. The dose rate averaged over an area at depth in the tissue is then calculated using Eq. [2.3]

$$\bar{D} = \frac{2\pi \int_0^R D(d')\, d'dd'}{\pi R^2} \qquad [2.3]$$

where *R* is the radius of the dose-averaging area.

The integration starts by choosing one of the eight elevation points (▲) in the source (Figure 2-4).

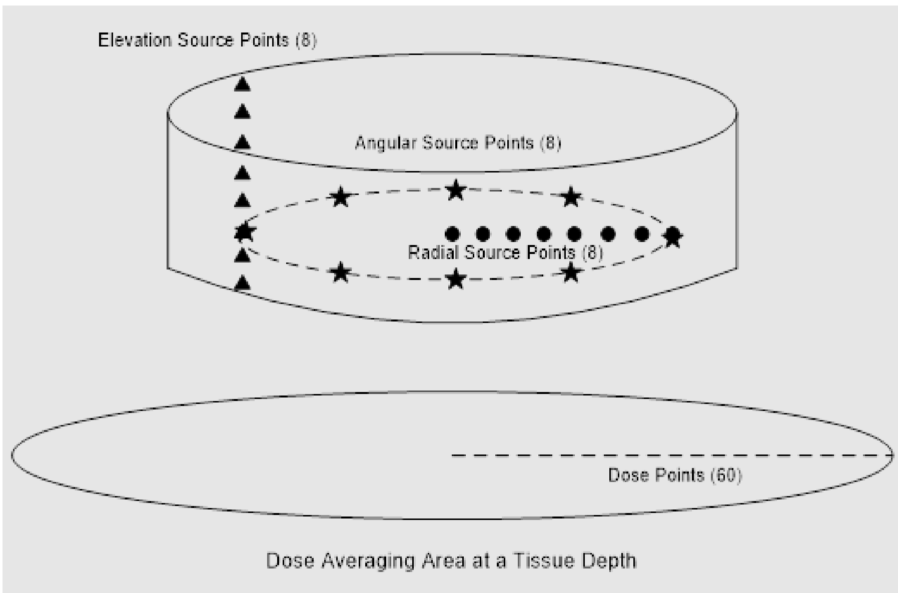

Figure 2-4. Schematic Representation of the Eight-Panel Quadrature Routine used to Calculate Dose for a Symmetric Source (redrawn from US NRC 2006)

At one of these elevations, one of eight concentric circles (radial source-points ●) is chosen. One of these circles is then subdivided into eight source-points at 45-degree angles from each other (angular source-points ★). Finally, the dose rate is calculated at each dose point from each of these eight source-points at a given elevation and radius. The contribution to the dose from the first four points is compared to the contribution of the last four points in each circle. If the relative difference between the two contributions is less than 0.01 percent, then convergence of the integral is achieved, and the procedure is repeated at the next radial position. If the relative difference between the two contributions is greater than the relative error, each of the two contributions is further subdivided into eight additional source-points, and the above procedure is repeated for each of the two sets of eight points. This process, known as the Newton-Cotes eight-panel quadrature routine, provides a fast and accurate method of numerically integrating complex functions such as DPKs (US NRC 1992; US NRC 2006; US NRC 2011).

2.1.3. Nonhomogeneous Dose-Point Kernels

DPKs from sources contained in a medium other than water (as a hot particle, for example) were also determined for 7.42 < Z ≤ 94 at 0.01 MeV ≤ E ≤8 MeV using EGSnrc Monte Carlo simulations, with identical transport parameters being applied. The intent of calculating these nonhomogeneous DPKs is to determine how energy is deposited in spherical shells of water after a monoenergetic electron has been emitted from the center of a sphere composed of a medium other than water. By determining the depth and energy-scaling parameters for this range of energies, it is possible to calculate the nonhomogeneous electron DPK for any known beta energy spectrum. This is accomplished by integrating over the electron energy spectrum for each source Z/thickness using Eq. [2.4]

$$\Phi_\beta(R,Z,\rho) = \frac{1}{E_{av}} \int_0^{E_{max}} ESP(R,E,Z,\rho)E\ N(E)\Phi(r,E)dE \qquad [2.4]$$

where r is the spherical shell radius, E_{max} is the endpoint energy of the beta spectrum, $N(E)dE$ is the fraction of electrons emitted per MeV per disintegration that have energies between E and $E + dE$. The average energy (Eq. [2.5]) is therefore

$$E_{av} = \int_0^{E_{max}} E\ N(E)dE \qquad [2.5]$$

For example, if the nuclide and source material in question are Co-60 and iron, the scaling parameters are used to create an n x m array of DPKs for ^{60}Co with source radii ranging from 0 to $\boldsymbol{a}\cdot X_{90}$ of iron and the water radii ranging from 0 to $\boldsymbol{b}\cdot X_{90}$ of water. The parameter ***a*** is based on complete electron energy absorption in the source material, and ***b*** is based on complete electron energy absorption in water when the source thickness is zero.

Nonhomogeneous beta-particle DPKs were determined by incorporating scaling equations into *SadCalc.exe*. The *SadCalc.exe* routine uses ICRP 107 (2008) electron emission spectra to calculate homogeneous water DPKs for each electron present in each dose calculation. Linear interpolation was used to accommodate all source media with 7.42 ≤ Z_{eff} ≤ 94.

Nonhomogeneous DPKs were calculated for a wide range of electron energies (Table 2-1) and source materials (Table 2-2). Stainless steel and uranium oxide were chosen as they represent common hot particle materials, and tungsten alloy was chosen to demonstrate the model's ability to handle high-density media.

Table 2-1. List of Nuclides used in Scaling and Scattering Models

Nuclide	$\overline{E}$ (MeV)	X_{90} (cm)
Co-60	0.0958	0.033
Sr-90	0.196	0.083
Bi-210	0.307	0.212
I-135	0.375	0.239
Sr-89	0.583	0.321
P-32	0.695	0.363
Mn-56	0.832	0.634
Y-90	0.934	0.533
Pr-144	1.217	0.696

Table 2-2. Source Materials used for Nonhomogeneous Electron DPK Testing

Alloy	Z_{eff}	Density (g/cm^3)
Stainless Steel (SS_302)	25.81	8.06
Tungsten Alloy (Mallory 2000)	72.79	18.00
Uranium Oxide	87.88	10.96

2.1.4. Backscatter Model

A volumetric backscatter model is used in SkinDose to predict the dose perturbations from both source and atmospheric backscattering. The model is applicable to electron-emitting radionuclides in a spherical, cylindrical and slab source geometry, and to source materials with $7.42 < Z_{eff} \leq 94$. Based on the DPK concept, SkinDose relies on the numerical integration of a point kernel over the source volume and the dose region of interest. The medium for which the DPK is defined is typically water, thus allowing for direct comparison with tissue. While the electron scattering contribution has been studied extensively for medical physics applications, it has been limited to point-source assumptions in the past yet has been expanded to volumetric sources for use in SkinDose. In addition to internal source scatter, electron scattering must also be considered in the medium surrounding the source (i.e., atmospheric scattering).

Air Backscatter Correction. Inherent in the development of electron DPKs is the assumption of an infinite homogeneous medium (water/water interface). The isotropic nature of DPKs assumes that electrons emitted away from the dose point can scatter back toward the dose point in an infinite homogeneous water medium and possibly contribute to dose at the point of interest. While scaling methods account for the nonhomogeneous media that transmit the electrons, an additional adjustment is required to correct for the lack of scatter since an atmospheric medium is above the skin rather than a modeled water medium (i.e., an air/water interface). In the situation of a source resting on the skin, the air above the source (air/water interface) results in less backscatter than would have been modeled in developing the DPKs. This scenario is of particular importance for hot particle skin dosimetry.

In the development of the electron dosimetry model (Mangini 2012), point-source planar dose profiles were determined using EGSnrc Monte Carlo simulations for the scattering media of water, air, and source materials with $7.42 < Z_{eff} \leq 94$ at electron energies of $0.01\ \text{MeV} \leq E \leq 8\ \text{MeV}$. The planar dose volumes were 1 mg cm^{-2} thick, with a maximum normal depth of 1,000 mg cm^{-2}. The dose-averaging areas were 1 cm^2 and 10 cm^2, and the scattering medium was assumed infinite (>> electron range) in both thickness and lateral extent.

In general, a backscatter factor is found by taking the ratio of the planar dose when the scattering material is present (nonhomogeneous case) to that when water is present (homogeneous case). Air scattering corrections often are reported inversely such that they are greater than or equal to one (1) (Cross et al. 1992). Regardless, these backscatter factors will be dependent on electron energy, the effective atomic number (Z) of the backscattering medium, normal depth, and dose-averaging area. When applied to an electron-emitting nuclide, the backscatter factor for a given dose-averaging area takes the form of Eq. [2.6]

$$B_{\beta}(Z,z) = \frac{\int_0^{E_{max}} D_{A,S}(Z,z,E)N(E)dE}{\int_0^{E_{max}} D_W(z,E)N(E)dE} \quad [2.6]$$

where z is the normal depth, D_W is the dose in the water/water geometry, $D_{A,S}$ is either the dose in the air/water geometry or the dose in the source/water geometry, and N(E) dE is the fraction of electrons emitted per MeV per disintegration that have energies between E and $E + dE$. Surface functions were used to determine monoenergetic electron planar dose profile curve fits for use in [2.6]. Once planar dose profile curve fits were determined, they were implemented in SadCalc.exe. The ICRP 107 (2008) electron-emission spectra were then used to calculate the electron backscatter factor of [2.6]. Linear interpolation was used for all $7.42 < Z \leq 94$.

SkinDose includes the ability to disable backscatter correction for electrons in air. Invoking the option to disable air backscatter correction sets all air backscatter correction to unity (1) so that no correction is made to electron scatter in air.

Source Backscatter Correction. It is important to remember that it is not possible to determine the absolute volumetric backscatter factor using the same procedures for point sources. This is due to the largely different energy-degradation properties of air and water and their impact on the respective dose calculations. Therefore, several assumptions and estimations were made.

The method is based on a selective integration process over the entire source volume. Rather than applying an overall correction factor to final dose calculations, scattering corrections are applied at each step of the numerical integration of dose. If desired, the "volumetric" correction factor could then be determined by taking the ratio of overall dose with the applied point-source scattering corrections to the overall dose without correction. Selection criteria are used to determine the proper type and amount of scattering correction for which to account. Scattering corrections are divided into three components: source/water interface corrections (for the top and bottom of the source), air/water interface corrections (for both the top and the sides of the source), and air/source interface corrections (for the sides of the source).

During the numerical integration process for an "infinitely large" source (dimensions > electron range), only source points positioned directly at the source/water interface (i.e., source/skin interface) will require the full application of the source/water scattering data (Figure 2-5). Source points positioned above this interface (Figure 2-6) require a more advanced treatment. In this case, there is expected to be an increase in the energy absorption (i.e., dose) from downward scattering occurring in the upper portion of the source, as well as a decrease in dose from upward scattering in the lower portion of the source. If the contribution from downward scattering is greater than the contribution from upward scattering, the dose will be increased for that source-point kernel. Likewise, when the upward contribution is greater, the dose will be decreased. This argument shows that when the source point is at the top of the source, the application of both air/water and source/water correction results in an effective air/source correction.

Scattering contributions from both upward and downward scattering are determined using [2.7]. The scattering material thicknesses for the top and bottom of the source are given by the normal distances from the source-point to the upper- and lower-most points of the source, respectively. The source backscatter correction factor (BSCF) is then determined by multiplying net scattering effectiveness by the electron source/water scattering correction for point sources,

$$Source\ BSCF_{top/bottom} = SW(SE_{top} - SE_{bottom}) \qquad [2.7]$$

where *SW* is the electron source/water scattering correction for point-sources, SE_{top} is the scattering effectiveness for the top portion of the source, and SE_{bottom} is the scattering effectiveness for the bottom portion of the source. The "skin depth" at which the scattering factor is determined accounts for the normal density thickness of both the source and tissue through which the electron must traverse.

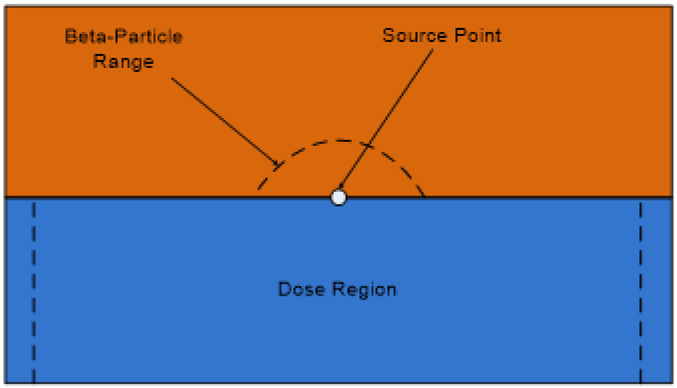

Figure 2-5. Schematic Demonstrating Conditions in Which Full Source/Water Scattering Corrections are Applied

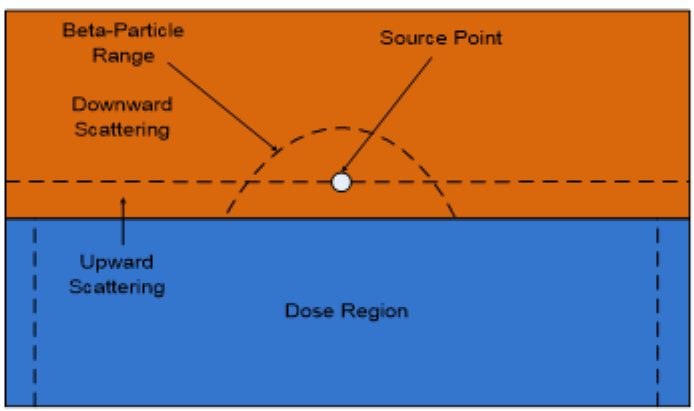

Figure 2-6. Schematic Demonstrating Conditions in Which Partial Source/Water Scattering Corrections are Applied

The point-source factors were developed with the assumption that the source medium is infinite in both height and lateral extent. As such, application to source points near or on the side of the source jeopardizes the accuracy of the results. However, approximations can be made to estimate source/scatter corrections for the sides of the source.

When the dimensions of the source are larger than the range of the electron, source points toward the center and the top-center of the source have minimal impact on dose. Therefore, source points on both sides and the bottom of the source become more important. It is estimated that scattering contributions from the sides of the source will reach a maximum when the scattering media thickness is 1.0 X/X_{90} and greater. Linear interpolation is used for X/X_{90} values less than 1.0.

Unlike source scattering for the top and bottom of the source, during the numerical integration process, the direction of the electron needs to be considered when correcting for side scatter. Side scattering is accounted for when the electron's path is directed away from the source and travels through air before reaching the dose region. The assumption is that an electron emitted in the 180-degree opposite direction would be permitted to backscatter off the source's side and still contribute to dose.

The amount of source material directly above the source point (considered the "lateral" dimension in this case) will also have an impact on the scattering effectiveness. If the source point is located on the top corner of the source, the probability of a backscattering event toward the dose region is greatly decreased. On the other hand, if the source point is at the bottom corner of the source, the probability of a backscattering event toward the dose region is much greater. It is estimated, therefore, that the normal distance to the uppermost point of the source must be greater than 0.5 X/X_{90} (or ½ of the "height" requirement) to have 100 percent scattering effectiveness from the top portion of the source. Therefore, the net scattering correction is given by Eq. [2.8]

$$Source\ BSCF_{side} = SA\frac{X_{top}}{0.5}(X_{op\_side} - X_{side}) \qquad [2.8]$$

where SA is the electron source/air scattering correction for point-sources (ratio of source/water to air/water correction factor), X_{side} is the normal distance to the side of the source through which the electron travels, X_{op_side} is the normal distance to the opposite side of the source, and X_{top} is the normal distance to the top of the source. All distances are relative to X90. If X_{top} is greater than 0.5, the full scattering correction is applied by setting X_{top} equal to 0.5. Similarly, if X_{side} or X_{op_side} is greater than 1.0, it is set equal to 1.0.

As the energy of the electron decreases and the scattered path angle relative to the air/water interface increases, the probability of the scattered electron depositing energy in the dose area greatly decreases (Figure 2-7). Conversely, high-energy electrons are expected to have a contribution extending to the edge of the dose area when scattered electrons enter the dose region at high incident angles. It is assumed that the scattering correction from the top and bottom of the source does not accurately account for such contributions because of its inherent geometry. Without knowing the angle at which a particular electron scatters and likely enters the dose region at each stage of the integration process, it is very difficult to correctly apply this additional correction factor. Therefore, the angle of incident (Figure 2-8) is used to estimate the frequency at which large angle scattering events occur. The side-scattering correction is applied only when the incident angle is greater than 70 degrees and when the density corrected path length (includes source and air) to the edge of the dose region, or the maximum scattered electron path length, is less than the electron X_{90} distance. The latter limitation prevents the side-scatter correction from being applied to low-energy electrons, where this form of scatter is believed unlikely (as explained above).

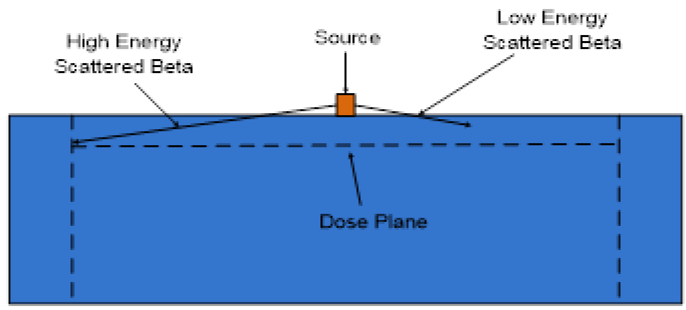

Figure 2-7. Schematic Illustrating Electron Energy Limitations of Side-Scatter Corrections

As with scattering from the top or bottom of the source, the “skin depth” at which the scattering factor is determined, considers the normal density thickness of both the source and tissue through which the electron must traverse.

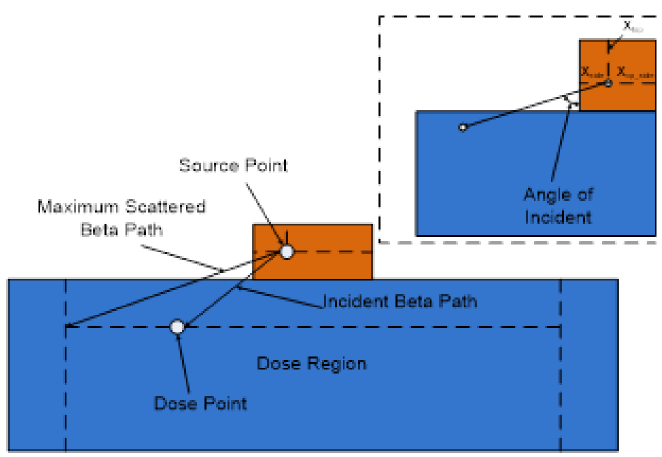

Figure 2-8. Schematic Illustrating Parameters used to Determine the Amount of Side-Scatter Correction Applied to High-Energy Electrons Emitted from Large Sources

The application of scattering correction factors is more difficult with an air/water interface than with a source/water interface. To estimate the scattering effectiveness when source material is present between the air/water interface, simple linear interpolation is used. The two extreme cases are when there is no source material between the air and water boundaries (Figure 2-9) and when the path length from the top or sides of the source is equal to or greater than the electron range. The scattering effectiveness would be 100 percent and 0 percent, respectively. The assumption is that if a backscattered electron can escape the source, there is a chance that a dose-contributing scatter event may still occur if water were surrounding the source. This is seen as a conservative estimate as an electron that travels 1.8 X/X_{90} (range estimate from US NRC 2006) out of the top of a source will theoretically not be able to backscatter and contribute to skin dose at any depth.

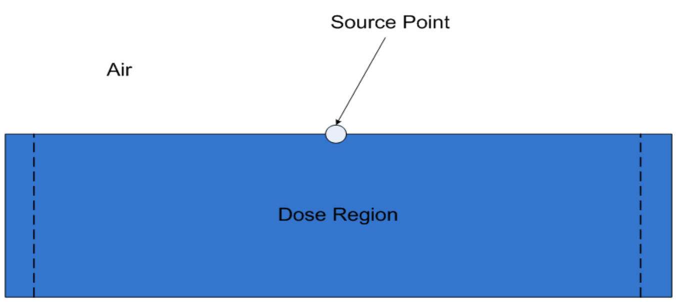

Figure 2-9. Schematic Demonstrating Conditions in Which Full Air/Water Scattering Corrections are Applied

The overall air BSCF is found using a weighted average. The BSCFs are calculated for all surfaces for which the electron can escape and reach air. Scattering contributions from the top of the source receive a 50 percent weight and the remaining 50 percent is evenly divided among the sides of the source. For cylinders and spheres, the shortest distance to the outer surface and the 180-degree opposite distance represent the two side distances (Figure 2-10). For slabs, four sides are used: the normal distances to the *x*-coordinate sides and the normal distances to the *y*-coordinate sides. The scattering reductions (for cylinders and spheres) are therefore given by Eqs. [2.9], [2.10], and [2.11]:

$$Air\ BSCF_{top} = AW\ 0.5\frac{1.8 - X_{top}}{1.8} \qquad [2.9]$$

$$Air\ BSCF_{side} = AW\ 0.25\frac{1.8 - X_{side}}{1.8} \qquad [2.10]$$

and,

$$Air\ BSCF_{op\_side} = AW\ 0.25\frac{1.8 - X_{op\_side}}{1.8} \quad [2.11]$$

where AW is electron air/water scattering correction for point sources, and X_{top}, X_{side}, and X_{op_side} are the distances to the top and sides of the source relative to X_{90}.

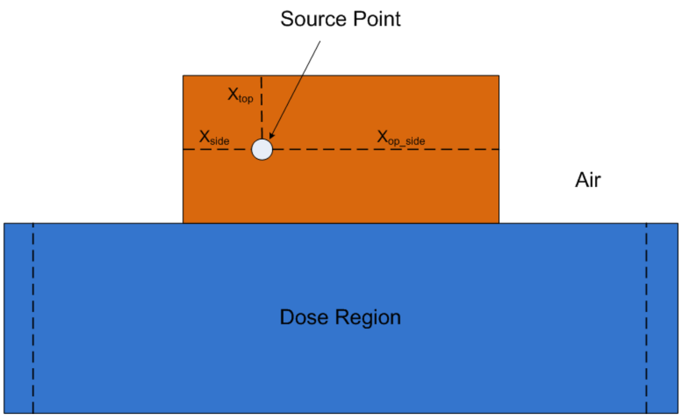

Figure 2-10. Schematic Demonstrating Conditions in Which Air/Water Scattering Corrections are Applied

Unlike the source scattering corrections, no depth adjustments need to be made for materials traversed by the electron before entering the dose region. This is because corrections are made for scattering events occurring outside the source. The distance to the air/water interface is considered negligible in terms of electron energy degradation (assumed to be completely air). The overall air scattering correction is found by summing the three components above.

All profiles were fit with a 28-parameter Chebyshev Series (LnX-Y, Order 6). While this is a complex fit equation, it allowed for all curves to be fit with the same functional form with a high goodness of fit ($R^2 > 0.999$). As an example, a second-order Chebyshev is given by Eq. [2.12]:

$$Z = a + bT_1(x') + cT_1(y') + dT_2(x') + eT_1(y') + fT_2(y') \quad [2.12]$$

where

$$x' = ln(x) = ln(Normal\ Depth\ (cm)) \quad \text{scaled -1 to +1,} \quad [2.13]$$

$$y' = y = ln(E\ (MeV)) \quad \text{scaled -1 to +1,} \quad [2.14]$$

$$T_n(x') = cos(\, n * a * cos(\, x')), \qquad [2.15]$$

and Z is the square root of the dose rate per particle (Gy Bq^{-1} s^{-1}).

Again, in SkinDose the ability to disable backscatter correction for electrons in the source is included. If source backscatter is disabled, no correction is made to electron scatter in the source.

2.1.5. Scaling Models

The DPK scaling model consists of two parameters: a depth-scaling parameter (DSP) and an energy-scaling parameter (ESP). Mangini and Hamby (2016) provide more detail.

Depth Scaling. The depth-scaling model begins with determining the range of the electron in both the homogeneous and nonhomogeneous geometries. Given the difficulty of determining an absolute electron range because of energy straggling and a torturous path, the spherical radius at which 99.0 percent energy deposition occurred was chosen as a range estimate. The difference in ranges between the homogeneous and nonhomogeneous data is therefore attributed to the absorption sphere in the nonhomogeneous case. For a given absorption radius, the resulting difference in ranges (Eq. [2.16]) is called the DSP,

$$DSP(R, E_0, \rho, Z) = X_{99\_H} - X_{99\_NH} \qquad [2.16]$$

where X_{99_H} is the homogeneous electron range, X_{99_NH} is the nonhomogeneous electron range, and ρ and Z are density and effective atomic number, respectively, of the absorption material.

As an example, consider an iron spherical source (r = 0.022 cm, Z = 26, ρ = 7.874 g/cm^3) and an electron energy of 1 MeV. The radius of the iron source was chosen to be 0.5 X_{90} to allow for sufficient electron self-absorption. Because of the presence of the 0.022 cm of iron, the electron range in the nonhomogeneous shells is 0.120 cm less than the homogeneous range (Figure 2-11). Therefore, for a 1 MeV electron traversing 0.022 cm of iron, the DSP will be 0.120 cm. Shifting the homogeneous DPK data to the left (i.e., degraded electron energy by self-absorption and therefore less skin penetration) by this amount will equate the ranges and provide the necessary depth adjustment (Figure 2-12).

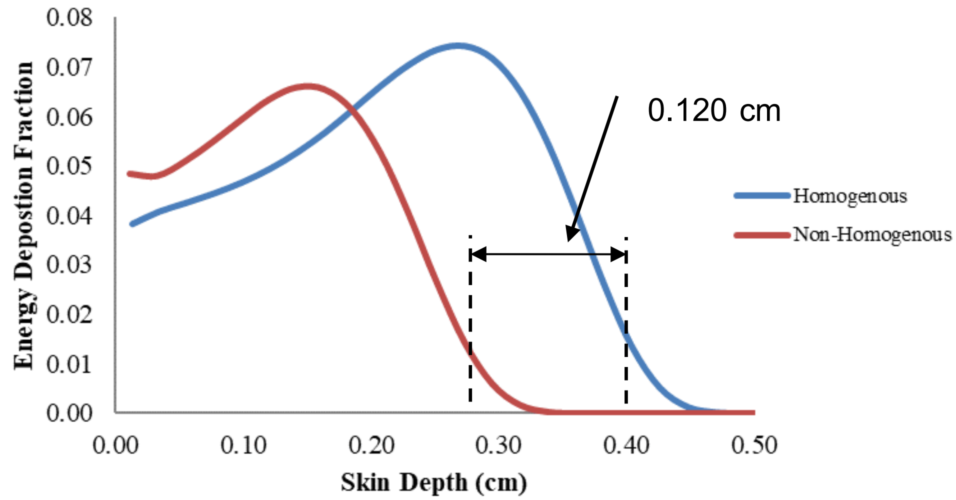

Figure 2-11. Comparison of 1 MeV Electron DPKs for the Homogeneous Water Case and the Case When the Electron Traverses an Iron Source of Thickness 0.022 cm

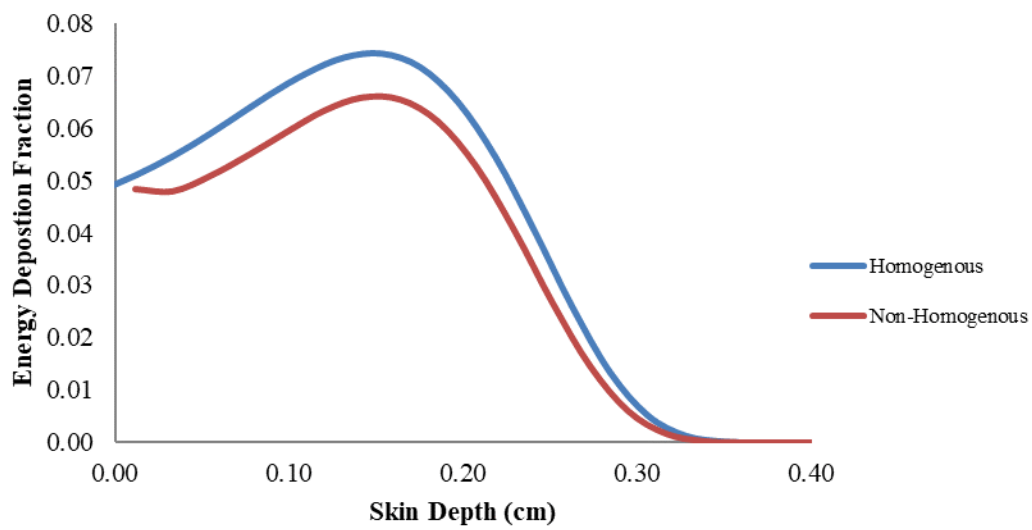

Figure 2-12. Example of Depth Scaling on the Homogeneous DPK Curve

When plotted together in three dimensions, the variability of depth scaling with respect to *Z* is difficult to discern, as all DSP factors follow the same curvature with little separation (Figure 2-12). The variation in *DSP*s at small radii is greatest, with essentially no variability at large radii. Each curve is linear with a slope near unity (1). This is expected since density thickness is often used to estimate "water equivalent" path length for electrons in nonaqueous media. The small Z dependence, coupled with 18 curve fits, allows for accurate interpolation for any $7.42 < Z \leq 94$.

All curve fits for the *DSP*s (Eq. [2.17]) took the following form:

$$LN(DSP\ (cm)) = \frac{(a + bx + cx^2 + dx^3 + ey)}{(1 + fx + gx^2 + hx^3 + iy)} \qquad [2.17]$$

where x is $LN(E\ (MeV))$ and y is $LN(X_x{*}\rho_x\ (g\ cm^{-2}))$. The terms X_x and ρ_x refer to the radius and density of the absorption sphere. The form of [2.17] was chosen because it was the equation that had the largest R^2 value (≥0.9999) and was able to fit all 18 plots. The fit parameters for each function demonstrated a slight Z dependence (Figure 2-13).

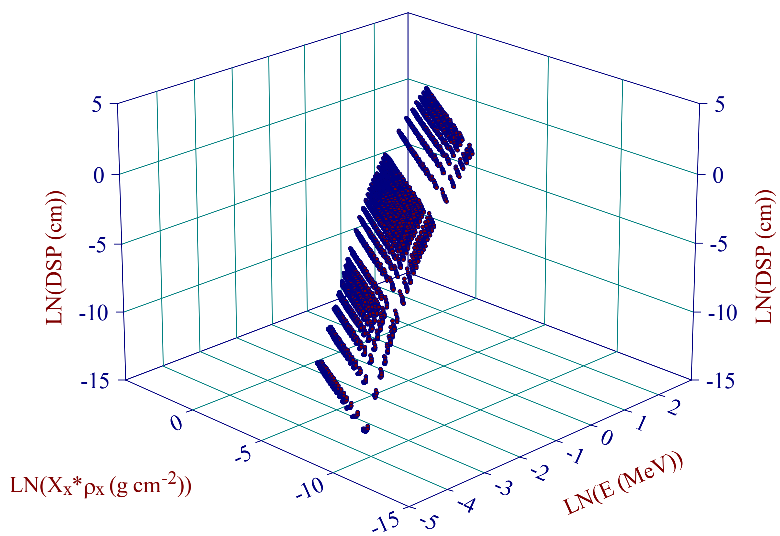

Figure 2-13. 3D Plot of Depth-Scaling Data for all Source Materials Modeled

Energy Scaling. The ESP is a direct result of energy conservation at distances within the electron's maximum range, or X_{99} (neglecting radiative loses beyond this distance). Once the homogeneous curve is shifted according to the DSP, the total energy deposition is found for each case. This is performed by summing the homogeneous DPKs for radii between the depth-scaling parameter and the X_{99} distance (Eq. [2.18]),

$$4\pi\rho \int_{DSP}^{X_{99}} r^2 \Phi(r, E_0)dr = E_{total} \qquad [2.18]$$

Similarly, the total energy deposition in the nonhomogeneous case is found by summing DPKs from 0 to X_{99}. The law of energy conservation requires the two to be equal. Therefore, the ESP is found by taking the ratio of the nonhomogeneous total to the homogeneous total (Eq. [2.19]),

$$ESP(R, E_0, \rho, Z) = \frac{4\pi\rho \int_0^{X_{99}} r^2 \Phi_{NH}(r, E_0) dr}{4\pi\rho \int_{DSP}^{X_{99}} r^2 \Phi_H(r, E_0) dr} \quad [2.19]$$

Applying the resulting ratio to the homogeneous DPK equates the total energy depositions in the two geometries. For the iron source example, an energy-scaling parameter of 0.887 is computed. Thus, energy conservation is achieved by multiplying the homogeneous curve by the ESP of 0.887 (Figure 2-14).

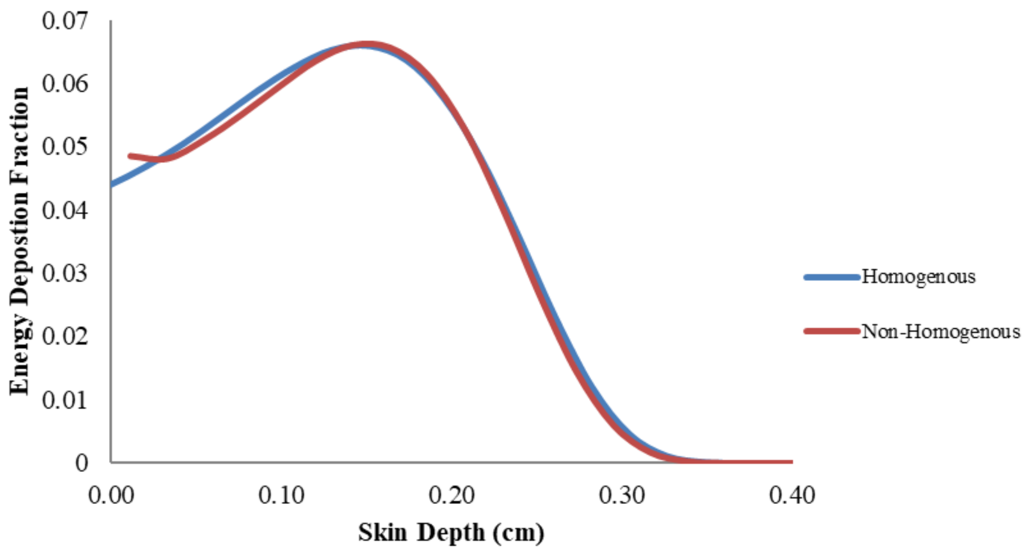

Figure 2-14. Example of Energy Scaling on the Homogeneous DPK Curve

As in the case of depth scaling, the natural logarithm of energy was used to decrease variability over the range of energies examined. The variability associated with the radius of the absorption sphere was minimized by expressing it as a ratio of density thickness to the X_{90} distance in water, $X_x{*}\rho_x$ / X_{90w}. The natural logarithm of the DSP multiplied by the initial electron energy, $LN(ESP{*}E_0)$, was chosen as the dependent variable. While the quantity of $ESP{*}E_0$ has no physical meaning, using it as the dependent variable produced better-fitting surface plots than simply using *ESP.* Since E_0 is a known quantity, solving for *ESP* is simple.

The variability of the *ESP* curves (Figure 2-15) with respect to Z is more pronounced than that of the *DSP* curves (Figure 2-13). The variation of *ESP*s becomes quite large as the absorption-sphere radius increases. As Z approaches that of water (Z_{eff} of 7.42), the *ESP* approaches 1.0, as expected. As Z increases, the amount of energy reduction following depth scaling increases. Once again, this is expected given the lower profile of high-Z nonhomogeneous DPK curves for the same absorption-sphere radius (with respect to X/X_{90}). Despite this increased variability, interpolation within surface plots is not seen as an issue.

All curve fits for the *ESP*s took the form (Eq. [2.20]):

$$LN(E * ESP\ (MeV)) = \frac{(a + bx + cx^2 + dx^3 + ey + fy^2)}{(1 + gx + hx^2 + iy + jy^2)} \quad [2.20]$$

where x is $LN(E\ (MeV))$ and y is $X_x * \rho_x / X_{90w}$. The terms X_x and ρ_x refer to the radius and density of the absorption sphere. The above equation was chosen because it had the largest R^2 value (≥0.999) and was able to fit all 18 plots. As with the *DSP*s, fit parameters demonstrated a slight Z dependence.

Integration of scaling parameters over a particular electron energy spectrum provides the nonhomogeneous DPK for a given source thickness. Comparisons with EGSnrc nonhomogeneous DPKs demonstrated excellent agreement over a range of electron energies and high-Z source materials by producing nearly identical DPKs for all absorption-sphere radii. In addition, when compared to Cross's (1992) scaling model and density scaling, the ability to account for spectral hardening is evident. This is largely because of the scaling model's ability to accurately calculate nonhomogeneous DPKs at each monoenergetic electron energy with a given emission spectrum.

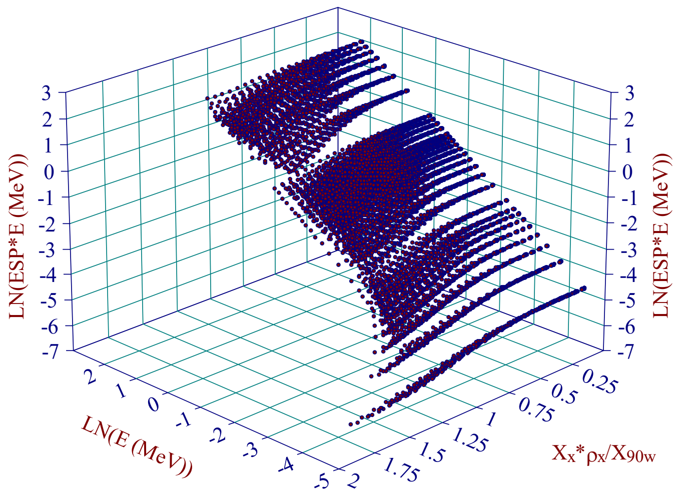

Figure 2-15. 3D Plot of Energy-Scaling Data for all Source Materials Modeled

2.1.6. Verification and Validation

To validate the new electron dosimetry models incorporated in SkinDose and previous versions of VARSKIN, results were compared to the general-purpose radiation transport codes, Monte Carlo N Particle (MCNP5) and EGSnrc. The two software packages are Monte Carlo transport codes that simulate interaction and transport of particles in material (Los Alamos National Laboratory, 2003; Ljungberg et al. 2012). The authors also compared VARSKIN 5.3 with results from various methodologies in the literature (Anspach and Hamby 2018). Since its unveiling in the late 1980s (US NRC 1987), VARSKIN results have been compared with those of many different authors. The following sections provide comparisons with former versions of VARSKIN so that the user can see how dose estimates have changed over the years. In addition, the reader will see comparisons with Monte Carlo simulations, as well as comparisons with results in the literature.

***Intercode Comparisons*.** The SkinDose electron dosimetry models have gone through extensive enhancements over their history. Comparisons of dose calculated using VARSKIN 4, 5.3, and 6.0 for point sources are given below (using ICRP 38 data for historical consistency) to demonstrate how the four versions differ in dose estimation for the few scenarios considered.

For point sources directly on the skin, calculations were made using several versions of VARSKIN for the case of a Co-60 point source (ICRP 107 decay data) placed directly on the skin (i.e., no material and no airgap between the source and skin). For a 37-kBq hot particle and a 1-hour exposure time, the electron dose averaged over 1 cm^2 at a depth of 7 mg/cm^2 was calculated. Table 2-3 shows the results of this calculation. Changes to electron dosimetry indicate a reduction of about 10 percent at this shallow depth, due primarily to changes in the calculation of specific absorbed dose distribution.

Table 2-3. Comparison of Electron Shallow Dose Estimates using VARSKIN 4, 5.3, 6.0, SkinDose 1.0, and 2.0 for a 37-kBq Point Source of Co-60 on the Skin for 1 hr

Nuclide	V4 (mGy)	V5.3 (mGy)	V6.0 (mGy)	SkinDose v1.0 (mSv)	SkinDose v2.0 (mSv)
Co-60	37.6	34.5	34.5	34	34

For point sources on cover material, dose calculations at 7 mg/cm^2 were also performed for Co-60, Cs-137/Ba-137m, and Sr/Y-90 with different cover material and airgap configurations. In each case, a 37-kBq point source and an exposure time of 1 hour were assumed with no gap between the layers of cover material. Doses were calculated for a 1-cm^2 averaging disk. Table 2-4 shows the results of these calculations. Changes to electron dosimetry are shown to either increase or decrease, because of model enhancements that affect particle track lengths, energy loss, backscatter characteristics, conversion electron consideration, and other factors.

Table 2-4. Comparison of Electron Shallow Dose Calculations from VARSKIN 4, 5.3, 6.0, SkinDose 1.0, and 2.0 for Various Cover Material Configurations

Nuclide	Airgap (cm)	Cover Material	V4 (mGy)	V5.3 (mGy)	V6.0 (mGy)	SkinDose v1.0 (mSv)	SkinDose v2.0 (mSv)
Co-60	0.2	M_1	1.96	2.17	2.17	2.2	2.2
Cs-137D	0.2	M_1	14.0	13.7	13.5	13	14
Sr-90D	0.2	M_1	32.6	29.1	28.2	28	29
Co-60	0.2	$2M_1$	0	0.0789	0.0789	0.077	0.081
Cs-137D	0.2	$2M_1$	4.75	6.50	6.44	6.4	6.6
Sr-90D	0.2	$2M_1$	20.7	19.5	19.1	19	19
Co-60	1.0	M_1	0.813	0.813	0.813	0.81	0.82
Cs-137D	1.0	M_1	2.79	2.59	2.53	2.5	2.6
Sr-90D	1.0	M_1	5.37	4.74		4.5	4.7
Co-60	1.0	$2M_1$	0	0.0409	0.0409	0.041	0.042
Cs-137D	1.0	$2M_1$	1.40	1.53	1.49	1.5	1.5
Sr-90D	1.0	$2M_1$	3.95	3.66	3.51	3.5	3.7
Co-60	1.0	$M_1 + M_2$	0	0.00838	0.00838	0.0078	0.0087
Cs-137D	1.0	$M_1 + M_2$	0.770	1.03	1.01	1.0	1.0

Sr-90D	1.0	$M_1 + M_2$	3.26	3.11	3.00	3.0	3.1
Co-60	5.0	$M_1 + M_2$	0	0.00045	0.00045	0.00043	0.00047
Cs-137D	5.0	$M_1 + M_2$	0.0384	0.0521	0.0513	0.051	0.053
Sr-90D	5.0	$M_1 + M_2$	0.167	0.158	0.153	0.15	0.16

Cs-137D includes the progeny Ba-137m; Sr-90D includes the progeny Y-90 (both in secular equilibrium with the parent).
M_1 — Cover material = thickness of 0.037 cm, density of 0.70 g/cm^3
$2M_1$ — Cover material = thickness of 0.074 cm, density of 0.70 g/cm^3
M_2 — Cover material = thickness of 0.040 cm, density of 1.1 g/cm^3

For an infinite plane electron source on the skin, calculations were performed for various nuclides using VARSKIN 4, 5.3, 6.0, and SkinDose to compare specifically the electron dose estimate for a large, distributed disk source (simulating an infinite plane) on the skin for an exposure period of 1 hour (Table 2-5). The electron dose at a depth of 7 mg/cm^2 was calculated for a simulated contamination scenario with a total activity of 3.7 MBq (37 kBq/cm^2) on a disk source with a diameter of 11.3 cm (100 cm^2). A dose-averaging area of 1 cm^2 was assumed.

Table 2-5. Comparison of VARSKIN 4, 5.3, 6.0, SkinDose 1.0, and 2.0 of the Electron Dose (mSv) for a 1-hr Exposure to an Infinite Plane Source on the Skin

Nuclide	V4	V5.3	V6.0	SkinDose v1.0	SkinDose v2.0
C-14	11.2	11.1	11.1	11	11
P-32	66.3	58.7	58.7	58	58
Co-60	37.7	34.5	34.5	35	35
I-131	52.4	48.4	48.4	48	48
Cs-137	51.2	47.8	47.8	48	48
Cs-137D	-	-	53.5	53	53
Sr-90	54.7	49.7	49.7	50	50
Y-90	68.3	59.7	59.7	59	59
Sr-90D	-	-	110	110	110

Cs-137D includes the progeny Ba-137m; Sr-90D includes the progeny Y-90; secular equilibrium assumed

Table 2-6 shows additional comparisons at various shallow depths in tissue for a source of yttrium-90 (Y-90).

Table 2-6. Dose (mSv) versus Depth for a 37 kBq/cm^2 Distributed Disk Source of Y-90 and a 1-hr Exposure Time (Dose Averaged over 1 cm^2)

Method	4 mg/cm^2	7 mg/cm^2	10 mg/cm^2	40 mg/cm^2
VARSKIN 4	79.0	68.3	61.4	40.7
VARSKIN 5.3	65.9	59.7	55.5	38.4

VARSKIN 6.0	65.9	59.7	55.5	38.4
SkinDose 1.0	64	59	54	38
SkinDose 2.0	65	59	55	38

Dosimetry Verification and Validation Using Monte Carlo Simulations. MCNP5 and EGSnrc were the two Monte Carlo simulation applications used to compare electron dose calculated in SkinDose. With each application, various source geometries were modeled close to the skin. The fundamental geometry involves an infinite volume of air located above an infinite volume of tissue. Composition of these materials was taken from NIST standards for each material. Each of the sources was situated 1 micron above the skin and above the perpendicular bisect of the volume of tissue over which the dose is calculated.

The dose per particle (electron) was calculated for each of the sources at tissue depths of 7, 100, 300, and 1,000 mg/cm^2. The density thicknesses of 7, 300, and 1,000 mg/cm^2 correspond to the depth required by 10 CFR Part 20, “Standards for protection against radiation,” for calculation of dose to the skin, lens of the eye, and the deep dose, respectively. Although the value of 100 mg/cm^2 does not correspond to a regulatory-significant density thickness, results at that depth are provided as an indication of accuracy at an intermediate, yet shallow, depth.

At each density thickness, the dose to two volumes of tissue, 0.002 cm^3 and 0.02 cm^3, was calculated. These dimensions correspond to cylindrical volumes within tissue, each having a thickness of 20 μm and a cross-sectional area of 1 cm^2 and 10 cm^2, respectively. The value of 20 μm was selected to create a volume large enough that uncertainties resulting from low numbers of particles interacting in the volume would not be an issue. Sherbini et al. (2008) showed that at thicknesses greater than 10 μm, any effects of dose-averaging over increasingly smaller volumes are avoided.

Energy deposited in the volume of interest was calculated for dose estimation. The number of particle histories executed was sufficiently high to maintain statistical errors below 6 percent, with the majority producing an error of approximately 3 percent. Dose rate was calculated for a simulated source strength of 37 kBq, with a yield of 100 percent at a given energy ranging from 0.025 to 3 MeV. While this is not specific to any nuclide, it demonstrates the energy dependence of each methodology and shows which models are accurate predictors as compared to Monte Carlo simulations. Previous versions of this document show results of electron dosimetry comparisons arranged in the following seven geometries: (1) point source; (2) 0.5 mm diameter 2D disk source; (3) 1 mm diameter 2D disk source; (4) 5 mm diameter 2D disk source; (5) 1 mm diameter by 1 mm height cylindrical source; (6) 1 mm diameter spherical source; and (7) 1 mm cube slab source. For each geometry, dose estimates from VARSKIN 5 as a function of electron energy were compared with EGSnrc and MCNP5 results at depths of 7, 100, 300, and 1,000 mg/cm^2. VARSKIN 5 estimates of dose compare very well with those from EGSnrc and MCNP5, although MCNP5 estimates are slightly higher at deeper depths. Finally, comparisons with four beta-emitting nuclides (Al-28, K-42, Cu-66, and Cs-138) were made to show how VARSKIN 5 electron dose predictions compare to VARSKIN 4 estimates.

For additional evidence on the efficacy of SkinDose, the user is directed to two publications in which VARSKIN 5.3 results are compared with historical literature on electron skin dosimetry (Anspach and Hamby 2018; Dubeau et al. 2018).

2.1.7. Limitations

As noted above, the SkinDose validation results indicated differences between VARSKIN 5 and EGSnrc for electron dosimetry in scenarios involving volumetric sources and intermediate electron energies. The validation results for low-energy electrons at shallow depths are similar to the results seen at all depths where the electron is reaching its maximum range (even for the point-sources to a certain degree). These larger deviations are apparent at the tail end of the electron-dose profiles, as well (Mangini, 2012). Either way, it is clear from these results that the accuracy of SkinDose decreases as the electron reaches its maximum depth. In dose calculations for a distribution of electrons, this effect is still present since, approaching the deeper depths, the deposited energy is occurring at the tail end of the electron range.

SkinDose has been shown to be reliable for particulate sources that have dimensions less than eight times the X_{99} distance of the radionuclide in tissue. The X_{99} distance is essentially 99 percent of the range of beta particles in tissue emitted by nuclides in the source term. When the physical size of the source approaches this value, SkinDose may give unreliable results. A user who wants to model sources larger than this limit may wish to begin with smaller sources and increase the source size gradually to ensure that spurious results are not being generated. Modeling a source of this size is generally not necessary, however, as most of the source does not contribute to electron skin dose because of self-shielding. If the source dimensions selected are too large, SkinDose warns the user of the potential for inaccurate results. The X_{90} distance is about 56% of X_{99}. X_{90} is included on the printout of a calculation to assist the user in determining the appropriateness of input source dimensions.

As a final note, SkinDose calculates shallow skin dose with the assumption that air is behind the source, i.e., an air/water (simulating tissue) interface at the skin surface. Users are reminded to take care when comparing SkinDose results to other calculations of skin dose that may have been executed with water behind the source (i.e., water/water interface). The BSCF used in SkinDose accounts for this interface difference.

DPKs and Scaling Model. DPKs have always underestimated dose at depths approaching the range of the electron. Monte Carlo is the standard and DPK models begin to fail when energy and range straggling become more and more important at greater depths. The effects of straggling are dominant at that part of the electron path. The authors suspect that the scaling model is not a contributor to the discrepancies noted. In fact, the accuracy of the scaling model is highest towards the end of the electron path. The interface between the source material and water is where the model has its largest deviations. This is likely not the cause, as electrons traversing very little of the source material (i.e., 0.25 X/X_{90}) will dominate the dose at deeper depths; the model is extremely accurate in this case.

Scattering Model. In developing the scattering model, the Monte Carlo (EGSnrc) data used for the model all had a standard error less than 5 percent. Simulations with a greater error were eliminated with a dose contribution of zero. However, once the curve fits in SadCalc.exe were developed for the dose profiles, the error in the predicted dose values from the curve fits became extremely unreliable at very low dose values and the deeper depths. In examining the raw data used to create the scattering model and dose profiles, it became apparent that the dose values reached an asymptote of about 1×10^{-12} (Gy per electron). At these dose values the standard error of the Monte Carlo simulations begins to exceed 5 percent. SkinDose was modified to set all dose contributions to zero if the calculation result was less than 1×10^{-12} Gy/electron. This patch is justified since the model begins to fail at such low doses. When averaging over a beta spectrum, these contributions to the BSCF and dose are negligible. Setting the dose to zero at these depths is executed for both the source scattering profile and the water scattering profile, thereby setting the BSCF equal to one (1). Nonetheless, for doses just greater than 1×10^{-12} Gy/electron, the SkinDose model will be rather inaccurate for dose calculations at depths near the end of the electron range.

2.2. Photon Dosimetry

The photon dosimetry model, first implemented in VARSKIN 4 (US NRC 2011), is an improvement to the basic photon model used in the VARSKIN 3 version. The model uses a point kernel method that considers the buildup of CPE, transient CPE, photon attenuation, and off-axis scatter. The photon dose model has many of the basic assumptions carried in the electron dosimetry model, namely that the source can be a point, disk, cylinder, sphere, or slab and that dose is calculated to an averaging disk immediately beneath the skin surface at a depth specified by the user. Photon dose is calculated for a specific skin averaging area, also specified by the user.

A major problem associated with deterministic photon dosimetry is determining the amount of charged-particle buildup and electron scatter within shallow depths. Federal U.S. law (10 CFR 20.1201(b)) states that a dose-averaging area of 10 cm^2 is appropriate for skin dosimetry specifically at the SDE depth of 7 mg/cm^2 in tissue). Throughout this section, the word "depth" is meant to indicate the distance from the skin surface to some point directly beneath a point source, normal to the skin surface.

To begin the explanation of the dose model, the simple instance of a volume of tissue exposed to a uniform fluence, Φ_0, of uncollided photons of energy, E, from a point source in a homogeneous medium is assumed. When attenuation is ignored and it is assumed that CPE is established, the dose to any and every point in that volume of tissue is (Eq. [2.21]):

$$D(E) = \Phi_0 \cdot E \cdot \left(\frac{\mu_{en}}{\rho}\right)_{tissue} \qquad [2.21]$$

where $\left(\frac{\mu_{en}}{\rho}\right)_{tissue}$ is the energy-dependent mass energy absorption coefficient for tissue. With this calculation of dose, it is essentially assumed that the tissue volume is infinitely thin and that interactions occur in two dimensions, normal to a beam of incident photons. The uncollided fluence originating from a point source (Eq. [2.22]) can be determined by:

$$\Phi_0 = \frac{S}{4\pi d^2} \qquad [2.22]$$

where *S* has units of photons emitted per nuclear transition (i.e., yield), and *d* is the distance between the source and dose locations, in an infinitely large homogeneous volume. Thus, a point-kernel tissue dose per transition at distance, *d*, from a point source (Eq. [2.23]) can be calculated for radionuclides emitting *i* photons of energy *E* and yield *y*, such that:

$$\text{Dose}\left[\frac{\text{Gy}}{\text{nt}}\right] = \frac{k\left[\frac{\text{J}\cdot\text{g}}{\text{MeV}\cdot\text{kg}}\right]}{4\pi d^2[\text{cm}^2]} \cdot \sum_i \left[y_i\left[\frac{\text{photon}}{\text{nt}}\right] \cdot E_i\left[\frac{\text{MeV}}{\text{photon}}\right] \cdot \left(\frac{\mu_{en}}{\rho}\right)_{i,tissue}\left[\frac{\text{cm}^2}{\text{g}}\right]\right] \qquad [2.23]$$

where $k = 1.602x10^{-10}\left[\frac{\mathrm{J \cdot g}}{\mathrm{MeV \cdot kg}}\right]$.

If the point source is assumed to rest on the skin surface (with a density interface), and a profile of dose with depth in tissue is of interest, Eq. [2.23] must be modified to account for the attenuation of photons in tissue, the electronic buildup, and electron scatter at shallow depths leading to CPE. First, given that attenuation is occurring as photons travel through tissue, photon fluence is decreasing by an attenuation factor ($e^{-\mu d}$) where μ is the energy-dependent linear attenuation coefficient for tissue. Interaction coefficients are taken from International Commission on Radiation Units and Measurements (ICRU) 44, "Tissue Substitutes in Radiation Dosimetry and Measurement" (ICRU 1989). Since tissue typically is assumed to be of unit density (1 g/cm^3), the value of μ (in units of cm^{-1}) is numerically identical to the value of μ/ρ (in units of cm^2/g).

To simplify software coding, analytical expressions are used in SkinDose (as opposed to using "lookup tables") for a number of dosimetry parameters. A highly accurate empirical relationship to estimate μ/ρ (in units of cm^2/g) for tissue as a function of incident photon energy (in units of MeV) was developed and is given below ([2.24]). The equation is appropriate for photon energies between 0.001 and 10 MeV.

$$\frac{\mu}{\rho}(E) = \frac{a_0 + \sum_{i=1}^{9} a_i \ln^i E}{1 + \sum_{i=1}^{7} b_i \ln^i E}. \qquad [2.24]$$

A similar function was developed ([2.25]) to approximate the energy-dependent value of μ_{en}/ρ for tissue, again appropriate for photon energies between 0.001 and 10 MeV;

$$\frac{\mu_{en}}{\rho}(E) = \frac{a_0 + \sum_{i=1}^{7} a_i \ln^i E}{1 + \sum_{i=1}^{8} b_i \ln^i E}. \qquad [2.25]$$

Table 2-7 provides the coefficients for the fit of Eqs. [2.24] and [2.25] to the ICRU 44 (1989) data.

In consideration of CPE, Attix (1986) states that the condition exists if, in an infinitely small volume, "…each charged particle of a given type and energy leaving [the volume] is replaced by an identical particle of the same energy entering." For dose at shallow depths to be accurate, the user must determine the degree (fraction) to which CPE, as a function of depth, has been achieved. The SkinDose estimation of the CPE fraction is based on Monte Carlo simulations and the difference between kinetic energy released in matter (KERMA) and energy absorbed (dose) as a function of depth.

Table 2-7 Function Coefficients

Coefficient	Eq. [2.24]	Eq. [2.25]
a_0	0.06997	0.03067
a_1	-0.004154	0.01285
a_2	-0.006919	-0.002061
a_3	0.001211	-0.001057
a_4	0.0005208	0.0003150
a_5	-0.00005960	0.0001143
a_6	-0.00002192	-0.00001012
a_7	0.0000007728	-0.000005314
a_8	0.0000007706	-
a_9	-0.00000002494	-
b_1	0.4296	0.5972
b_2	0.03627	0.1361
b_3	-0.005849	0.01239
b_4	-0.000006259	-0.0006503
b_5	0.0003312	-0.0003667
b_6	0.00004527	-0.00005769
b_7	0.000001844	-0.000004669
b_8	-	-0.0000001555

Since energy transfer (i.e., KERMA) from photons and energy absorption (i.e., dose) from the resulting charged particles do not occur in the same location (Johns and Cunningham, 1983), there is a "buildup region" in which dose is zero at the skin surface and then increases until a depth is reached at which dose and KERMA are essentially equal. The depth at which equilibrium occurs is approximately equal to the range of the most energetic electron created by the incident photons (Johns and Cunningham, 1983). The authors determined an energy-dependent factor accounting for CPE buildup (f_{cpe}) by Monte Carlo simulation (using MCNP5); this factor (Eq.[2.26]) is the ratio of dose, *D*, to KERMA, *K*, for a particular incident photon energy at a given tissue depth;

$$f_{cpe}(E,d) = {}^{D}\!/_{K} \qquad [2.26]$$

When considering CPE and attenuation, a relationship is achieved with depth in a medium in which dose is proportional to KERMA (Attix 1986); this relationship is referred to as transient charged particle equilibrium (TCPE). Dose reaches a maximum "at the depth where the rising slope due to buildup of charged particles is balanced by the descending slope due to attenuation" (Attix 1986), and then dose continues to decrease with depth because of subsequent attenuation of photons. At the point where TCPE occurs, dose is essentially equal to KERMA for low-energy photons and the value of f_{cpe} is equal to unity (1). As photon energy increases over about 1 MeV, this assumption of dose and KERMA equality begins to fail, but not so significantly that it appreciably affects dose estimations at depth. Based on experience with the Monte Carlo simulation of shallow and deep depths, the model used in SkinDose limits the value of f_{cpe} to 1.05 (i.e., it allows dose to exceed KERMA by no more than 5 percent at depth).

A function for f_{cpe} that is dependent on initial photon energy (Eq. [2.27]) is given as,

$$f_{cpe}(x) = \frac{1}{a + b \cdot ln(x) + {}^{c}/_{\sqrt{x}}} \qquad [2.27]$$

where x (in cm) is a function of energy and is equal to the point kernel distance between source point and dose point, and the coefficients a, b, and c are functions of energy (in keV) as described below:

$$a = 19.78 + 0.1492\ ElnE - 0.008390\ E^{1.5} + 0.00003624\ E^2 + 3.343\ \sqrt{E}lnE - 10.72\ {}^{E}/_{lnE} \qquad [2.28]$$

$$b = 1.217x10^{-12}E^4 - 5.673x10^{-9}E^3 + 7.942x10^{-6}E^2 - 0.002028E + 0.3296 \qquad [2.29]$$

$$c = 9.694x10^{-13}E^4 - 4.861x10^{-9}E^3 + 7.765x10^{-6}E^2 - 0.001856E + 0.1467 \qquad [2.30]$$

The f_{cpe} factor is used for all materials; any buildup for photon dosimetry in air or thin covers is expected to be insignificant as compared to tissue.

2.2.1. Integration Methods

As stated above, Federal law currently requires the determination of shallow dose to skin averaged over an area of 10 cm^2 at a depth in tissue of 7 mg/cm^2. To determine average photon dose at depth from a source at the surface, Eq. [2.23] must be integrated over the averaging area. Integrating the exponential, however, results in a solution with imaginary components. Therefore, a stepwise numerical integration of Eq. [2.23] is necessary, essentially providing an average of the point-kernel dose over combinations of photon emission locations within the volume of the radioactive source and dose point locations within an infinitely thin disk of tissue at depth, *h*, from the surface.

Studies were conducted to determine which numerical integration method achieved convergence most rapidly (i.e., dividing the dose-averaging disk into the fewest number of segments) for photon dosimetry. The studies investigated three segmenting methods (Figure 2-16): (1) segments determined by equal radii of the dose-averaging disk; (2) segments determined by equal off-axis angles; and (3) segments determined by equal annular area.

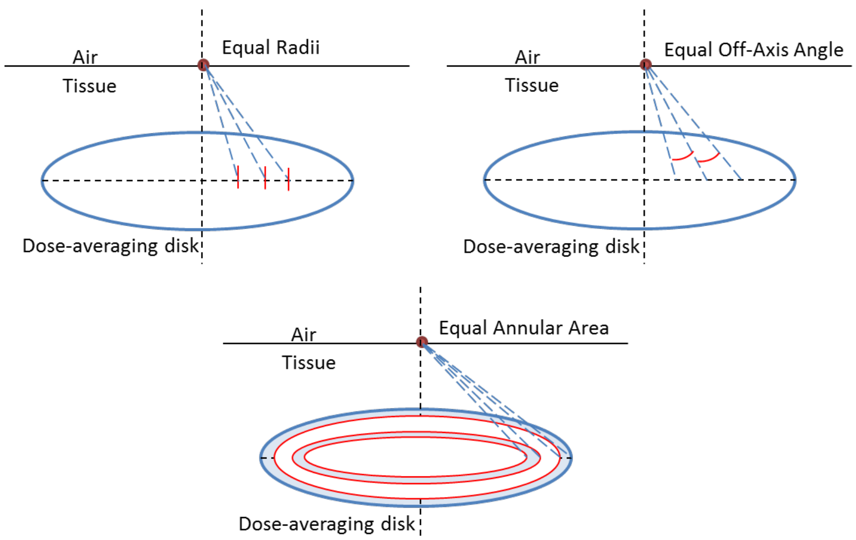

Figure 2-16. Depiction of Methods for Determining Integration Segments of the Dose-Averaging Disk

These studies indicate that segments divided according to equal lengths (radii) along the radius of the averaging disk converged with the fewest number of iterations, with segments divided by equal annular area requiring the most iterations. Figure 2-17 shows that convergence was achieved within about 300 iterations for equal lengths along the radius of a 10-cm^2 averaging disk; the SkinDose numerical integration, therefore, uses 300 segments along the radius or diameter. Convergence was achieved with fewer segments when analyzing a smaller averaging disk.

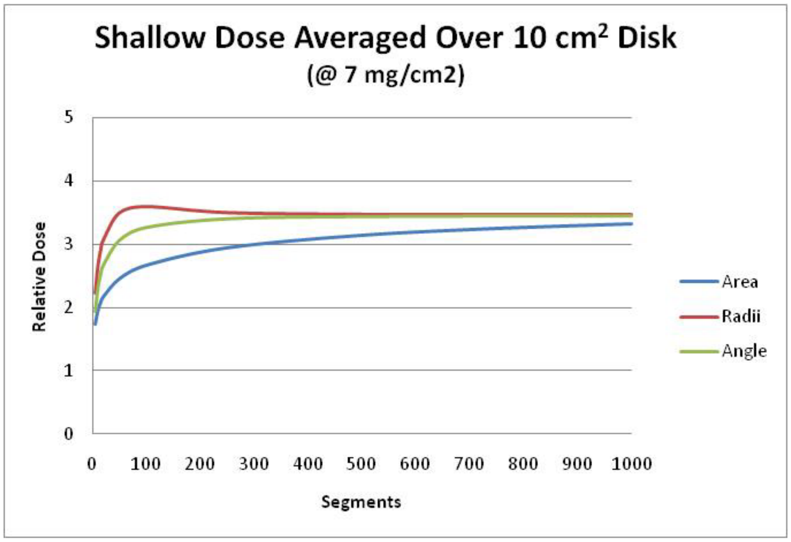

Figure 2-17. Relative Dose as a Function of the Number of Segments in a Numerical Integration (Iterations), by Method

Therefore, given a point source on the skin, the first task in the integration process is to divide the dose-averaging disk into *N* small segments (annuli), *j*, of uniform incremental radii. If an averaging area, *A*, of radius, *R*, is at some depth, *h*, beneath the surface of skin, a method based on the convergence study is used in which values of radii, R_j, of the averaging disk are selected such that a radial increment, Δr, is defined (Eq. [2.31]);

$$\Delta r = \frac{R}{N} \tag{2.31}$$

and

$$R_j = \sum_{j=0}^{N} (j \cdot \Delta r) \tag{2.32}$$

If point-kernel dose calculations are conducted where dose is estimated to the midpoint of the annulus, each dose must be weighted by w_j (Eq. [2.33]), the ratio of the annular area to the total area of the disk. Given that R_0 = 0 and R_N = *R*, the values of w_j are determined by:

$$w_j = \frac{R_j^2 - R_{j-1}^2}{R^2} \tag{2.33}$$

where *j* takes on values from 1 to *N*. Representing the average of the two radii describing the annulus in each calculation, r_j is defined by Eq. [2.34]:

$$r_j = \frac{R_j - R_{j-1}}{2} \tag{2.34}$$

Once all weighting factors are determined, then the dose per nuclear transition for a given point source radionuclide with *i* emissions, averaged over an infinitely thin disk of radius *R*, at normal depth in tissue *h* and radius r_j, is calculated by Eq. [2.35];

$$\dot{D}(h,R)\left[\frac{\text{Gy}}{\text{nt}}\right] = \frac{k}{4\pi}\cdot\sum_{j=1}^{N}\frac{w_j}{d_j^2}\left[\sum_i\left[y_i\cdot E_i\cdot\left(\frac{\mu_{en}}{\rho}\right)_i\cdot\left(f_{cpe}\right)_{i,j}\cdot\left(F_{oa}\right)_{i,j}\cdot e^{-\mu_i d_j}\right]\right] \tag{2.35}$$

where $d_j = \sqrt{\left(h^2 + r_j^2\right)}$.

2.2.2. Attenuation Coefficients for Cover Materials

For the selection of attenuation coefficients in photon dose calculations, the cover materials are “forced” to be either latex or cotton. This determination is made by the density entry, i.e., if the density is less than or equal to 1.25 g/cm^3, then latex is assumed, but if the density is greater, cotton is assumed. These are the two most likely materials used for cover. For photons, cover attenuation is relatively minor, and this assumption should be insignificant for the dose calculation.

An empirical function of energy for attenuation coefficients for cotton and latex is used, namely:

$$\mu = e^{(a + b\sqrt{E}\cdot\ln(E) + c\sqrt{E})} \tag{2.36}$$

Coefficients for air were determined from:

$$\mu_{air} = \left(\left(a + \frac{b}{\sqrt{E}}\right) + \left(c\cdot\frac{\ln(E)}{E}\right) + \left(\frac{d}{E}\right) + \left(\frac{e}{E^{1.5}}\right) + \left(f\cdot\frac{\ln(E)}{E^2}\right) + \left(\frac{g}{E^2}\right)\right) * 0.001168 \tag{2.37}$$

Table 2-8 contains the coefficients for each equation. Both functions track very closely with data from ICRU 44 (1989).

Table 2-8. Coefficients for Eqs. [2.36] and [2.37]

Coefficient	Cotton	Latex	Air
a	-0.10132	-1.0286	0.027413
b	0.31505	0.32189	-0.12826
c	-1.6086	-1.6217	0.11227
d	-	-	0.060526
e	-	-	0.12508
f	-	-	-0.0030978
g	-	-	-0.021571

2.2.3. Off-Axis Calculation of Dose

The model described thus far is constructed under the assumption that the source of photons is a point, located directly above and on axis with the averaging disk, and that there is symmetry in dose calculations along its radius. Dose to the averaging area is calculated for each of 300 annuli defined by radii r_{i-1} and r_i (Figure 2-18) weighted by the annuli area relative to total area.

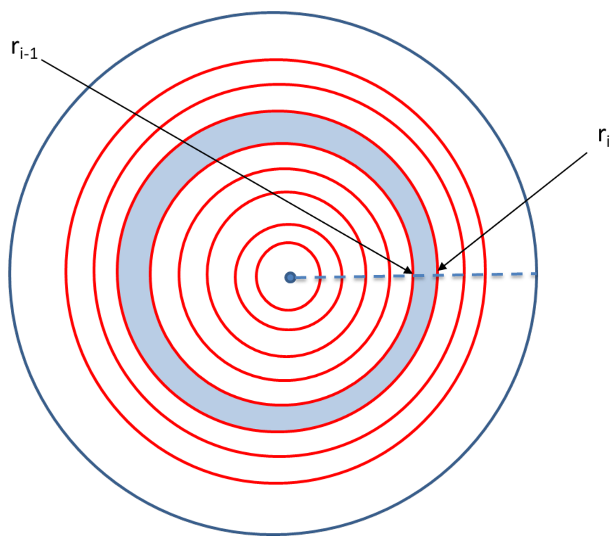

Figure 2-18. Dose-Averaging Disk with the Source Point Located on Axis

To extend the model to handle point-kernel calculations for volumetric sources, or for multiple point sources, the case where the point source is off axis yet still over the dose-averaging disk (Figure 2-19 and Figure 2-20) and the case where the point source is completely removed from the dose-averaging disk (Figure 2-21 and Figure 2-22) must be considered. The implication is simply a geometric determination of the distance between source and dose points in each point-kernel calculation and an area-weighted factor for the symmetric dose location on the averaging disk.

In the first case, where the point source is off axis yet still over the dose area, there is symmetry along a diameter of the dose-averaging disk. The average of the point-kernel doses will be determined by a weighting of dose calculated along the diameter. The calculation begins by projecting the dose point to the averaging disk, normal to the skin surface (see Figure 2-19).

The averaging disk then is divided, as described above, into a series of concentric annuli, about the projected dose point, until the radius of the annuli reaches the nearest edge of the averaging disk (Figure 2-20). At this point, the weighting model transitions to a series of arcs passing through the averaging disk; these arcs are created by differential radii of two intersecting circles (Figure 2-21). The model creates a total of 300 annuli and arcs. Point kernel dose is calculated along the diameter in each of the 300 segments defined by the differential annuli and arcs and then weighted based on the fractional area of each segment.

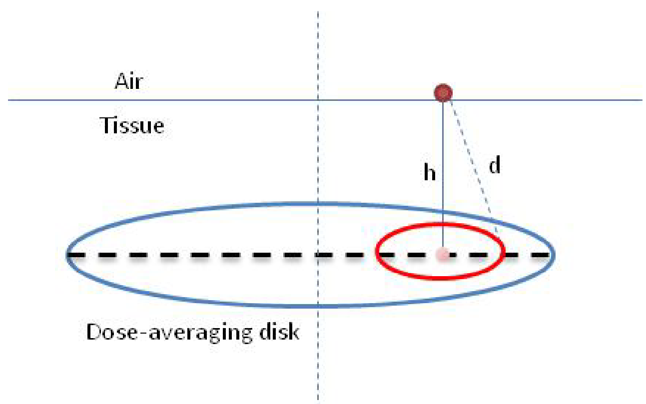

Figure 2-19. Dose-Averaging Disk Located at Depth h Beneath an Offset Point Source

The weight, or fractional area, of each annulus to the total is straightforward Eq. [2.38]), in that,

$$w_i = \frac{\pi\left(r_i^2 - r_{i+1}^2\right)}{\pi R^2} = \frac{r_i^2 - r_{i+1}^2}{R^2} \qquad [2.38]$$

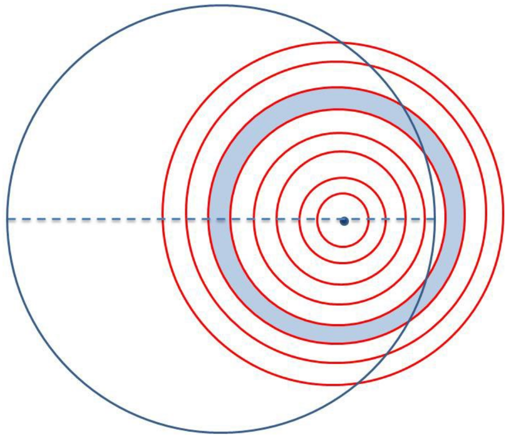

Figure 2-20. Dose-Averaging Disk with the Source Point Located Off Axis, yet Still Over the Averaging Disk

The weight of each arc is determined by a method considering intersecting circles. In the case of Figure 2-21, the area of the “lens” created by the two intersecting circles is given by Eq. [2.39]:

$$A_i = r^2 cos^{-1}\left(\frac{d^2 + r^2 - R^2}{2dr}\right) + R^2 cos^{-1}\left(\frac{d^2 + R^2 - r^2}{2dR}\right) - \frac{1}{2}\sqrt{(-d + r + R)(d + r - R)(d - r + R)(d + r + R)} \quad [2.39]$$

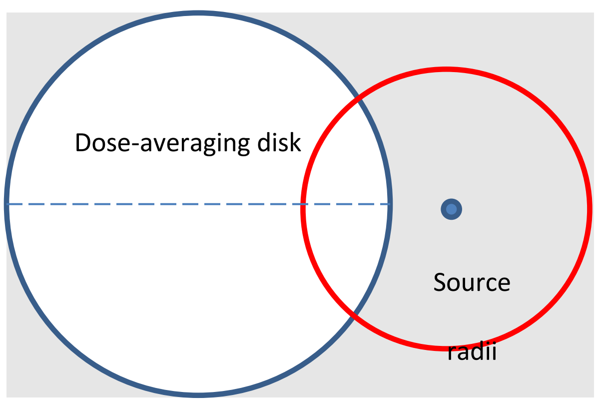

Figure 2-21. Relationship Between the Source-Averaging Disk and One of the Radii for dose Calculation

The area of the arc formed (Figure 2-22) by two concentric circles (two radii from the point source) that overlap another circle (the averaging disk) is the difference in the area calculations of Eq. [2.39]. The arc weight is then the ratio of the arc area to the total area of the averaging disk. In the case where the source projection does not fall on the dose-averaging disk (Figure 2-22), the weighting scheme is based solely on arcs.

The numerical integration is conducted from the point source to each of 300 locations along the diameter of the averaging disk (or along the radius if the source point is directly on axis with the disk). Then, for volumetric sources, point source locations are chosen in equal symmetric increments at fifteen locations in each of the three dimensions within the source volume, relative to the averaging-disk diameter. For each volumetric source dose estimate, 1,000 calculations of dose from each of 15 x 15 x 15 source point locations are executed (1 million dose calculations).

The SkinDose photon dosimetry model accounts for attenuation in cover materials and in air. As with the electron dosimetry model, up to five layers above the skin are allowed, with the air layer only acceptable just above the skin surface. For photon calculations, the material layers are restricted to cotton, latex, or both (by way of attenuation coefficient), and the source material is assumed to have the same characteristics as air. This latter assumption is not significant for very small volumetric sources and for photon energies above about 50 keV. For example, an examination of the ratio of air attenuation to lead, tin, copper, aluminum, and water attenuation, the greatest difference is obviously at low photon energies with higher-Z materials (i.e., instances of higher interaction probability).

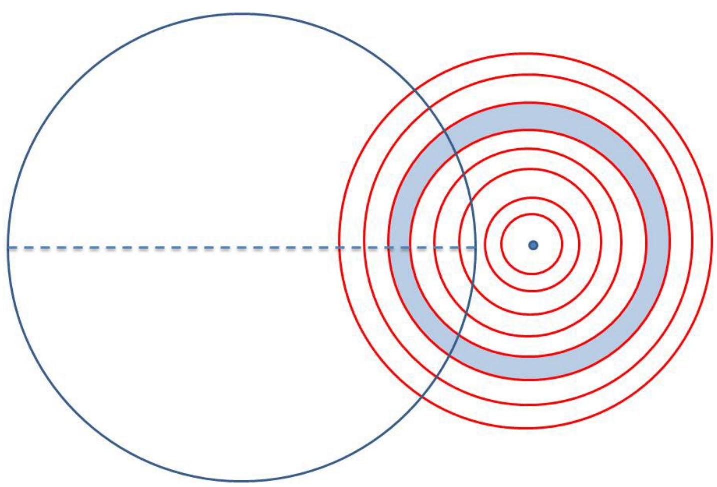

Figure 2-22. Dose-Averaging Disk from Above with the Source Point Located Off Axis, far Enough Removed to be Off the Averaging Disk

The data indicate that, for volumetric sources with a maximum linear dimension less than about 100 microns, the assumption that the source material is similar to air is of no consequence whatsoever for photon energies above 10 keV. As the source particle dimensions increase in size, an assumption of air for the source material can be quite significant for very low photon energies (< 40 keV). The significance, however, is one of conservatism in that more low-energy photons than actual will be modeled as striking the skin surface when source dimensions are large. This analysis also shows that, in terms of attenuation, the assumption of air and water (tissue) being similar over very short distances (< 5 mm) is valid.

2.2.4. Verification and Validation

Verification. A hand calculation (see Table 2-9) was performed using the decay chain of thorium-232, with an ingrowth time of 2 years and an exposure time of 5 hours. The Bateman equation was calculated via an Excel spreadsheet for six total timesteps (t + 0, 1, 2, 3, 4, and 5 hours after the 2-year ingrowth), then integrated using the trapezoidal method. The integrated activities and activity ratios so calculated are given below.

Table 2-9. Integrated activities and decay factors calculated manually for the Th-232 decay chain.

Nuclide	Activity (Bq) at T=0	Integrated Activity (nt)	Activity Ratio
Th-232	1.00	1.80e4	1
Ra-228	2.14e-1	3.86e3	2.14e-1
Ac-228	2.14e-1	3.85e3	2.14e-1
Th-228	6.40e-2	1.15e3	6.40e-2
Ra-224	6.32e-2	1.14e3	6.32e-2
Rn-220	6.32e-2	1.14e3	6.32e-2
Po-216	6.32e-2	1.14e3	6.32e-2
Pb-212	6.31e-2	1.14e3	6.31e-2
Bi-212	6.31e-2	1.14e3	6.31e-2
Po-212	4.04e-2	7.28e2	4.04e-2
Tl-208	2.27e-2	4.08e2	2.27e-2

Initial dose rates (in mSv/hr) for each of the necessary progeny nuclides were calculated (Table 2-10) using VARSKIN 6.2.1, V+ v1.2, and V+ v2.0, separated by electron, photon, and alpha dose (except V6.2.1, which does not have an alpha dosimetry model). Instantaneous dose rate results presented in SkinDose (and WoundDose) for decay chains includes only the parent nuclide since decay time is zero and no ingrowth has occurred.

Dose rates left blank in Table 2-10 indicate an emission that is not present for the given nuclide; dose rates listed as zero are calculated to be zero. Scenario parameters were left essentially at their default value (effective Z of 7.42, point source, no covers or air gap, 10 cm^2 averaging area, and 7 mg/cm^2 dose depth) for direct comparison.

Table 2-10. Initial dose rates for each member of the Th-232 decay chain, calculated individually in VARSKIN

Nuclide	VARSKIN 6.2.1 Initial Dose Rate (mSv/hr)		VARSKIN+ 1.2 Initial Dose Rate (mSv/hr)			VARSKIN+ 2.0 Initial Dose Rate (mSv/hr)		
	Electron	Gamma	Electron	Gamma	Alpha	Electron	Gamma	Alpha
Th-232	5.08E-08	1.68E-07	3.01E-08	1.97E-07	0.00E+00	3.01E-08	1.97E-07	0.00E+00
Ra-228	0.00E+00	3.80E-07	0.00E+00	3.89E-07		0.00E+00	3.89E-07	
Ac-228	1.77E-04	2.27E-06	1.72E-04	2.52E-06		1.72E-04	2.52E-06	
Th-228	5.69E-06	2.11E-08	5.68E-06	2.52E-07	0.00E+00	5.68E-06	2.52E-07	0.00E+00
Ra-224	0.00E+00	4.88E-08	1.98E-06	5.75E-08	0.00E+00	1.98E-06	5.75E-08	0.00E+00
Rn-220	0.00E+00	0.00E+00	0.00E+00	1.70E-09	0.00E+00	0.00E+00	1.70E-09	0.00E+00
Po-216	0.00E+00	0.00E+00	0.00E+00		0.00E+00	0.00E+00		0.00E+00
Pb-212	1.78E-04	1.04E-06	1.78E-04	1.12E-06		1.78E-04	1.12E-06	
Bi-212	1.01E-04	2.82E-07	9.99E-05	4.25E-07	0.00E+00	9.99E-05	4.25E-07	0.00E+00
Po-212	0.00E+00	0.00E+00			3.15E-01			2.58E-01
Tl-208	1.72E-04	3.71E-06	1.72E-04	3.79E-06		1.72E-04	3.79E-06	

To validate the new photon dosimetry models incorporated into SkinDose and previous versions, results were compared to the general-purpose Monte Carlo radiation transport code MCNP5, which simulates interaction and transport of particles in material (Los Alamos National Laboratory 2003; Ljungberg et al. 2012). VARSKIN 5.3 results were also compared with those from various methodologies in the literature (Anspach and Hamby 2018). Since the unveiling of VARSKIN (SkinDose) in the late 1980s (US NRC 1987), its results have been compared with those of many different authors. The following sections provide comparisons with former versions of SkinDose so that the user can see how dose estimates have changed over the years. In addition to seeing comparisons with Monte Carlo simulation, the reader will be directed to comparisons with the literature.

***Intercode Comparisons*.** The SkinDose photon dosimetry models have gone through extensive enhancements over the past several years. Comparisons of dose calculated using VARSKIN 4, 5.3, 6.0, SkinDose 1.0, and 2.0 for point sources are given below, using ICRP 38 (1983) data for historical consistency, to demonstrate how the four versions differ in dose estimation for the few scenarios considered.

For point sources directly on the skin, calculations were made using several versions of SkinDose for the case of a Co-60 point source placed directly on the skin (i.e., no material and no airgap between the source and skin). For a 37-kBq hot particle and a 1-hour exposure time, the photon dose was calculated averaged over 1 cm^2 at a depth of 7 mg/cm^2. Table 2-11 shows the results of this calculation. Photon dose estimates are consistent among recent versions with the inclusion of charged particle buildup and photon attenuation.

Table 2-11. Comparison of Photon Shallow Dose Estimates using VARSKIN 4, 5.3, 6.0, SkinDose 1.0, and 2.0 for a 37-kBq Point Source of Co-60 on the Skin for 1 hr

Nuclide	v4 (mGy)	v5.3 (mGy)	v6.0 (mGy)	SkinDose v1.0 (mSv)	SkinDose v2.0 (mSv)
Co-60	0.790	0.790	0.790	0.79	0.79

For point sources on cover materials, dose calculations at 7 mg/cm^2 were also performed for Co-60 and Cs-137/Ba-137m with three different cover material and air gap configurations (Table 2-12). In each case, a 37-kBq point source and an exposure time of 1 hour were assumed with no gap between the layers of cover material. Doses were calculated for a 1-cm^2 averaging disk. Table 2-12 shows the results of these calculations. Photon dose at shallow depths for the two radionuclides differed by about a factor of two, primarily due to the consideration of charged particle buildup and photon attenuation. For the same radionuclide, consistent results were obtained among recent versions.

Table 2-12. Comparison of Photon Shallow Dose Calculations from VARSKIN 4, 5.3, 6.0, SkinDose 1.0, and 2.0 for Various Cover Material Configurations

Nuclide	Airgap (cm)	Cover Material	V4 (mGy)	V5.3 (mGy)	V6.0 (mGy)	V+ v1.0 (mSv)	V+ v2.0 (mSv)
Co-60	0.2	M_1	0.292	0.290	0.292	0.29	0.29
Cs-137D	0.2	M_1	0.0969	0.0959	0.0917	0.099	0.099
Co-60	0.2	$2M_1$	0.258	0.257	0.258	0.26	0.26
Cs-137D	0.2	$2M_1$	0.0842	0.0834	0.0797	0.086	0.086
Co-60	1.0	M_1	0.0429	0.0427	0.0429	0.043	0.043
Cs-137D	1.0	M_1	0.0129	0.0128	0.0122	0.013	0.013
Co-60	1.0	$2M_1$	0.0404	0.0402	0.0404	0.040	0.040
Cs-137D	1.0	$2M_1$	0.0121	0.0121	0.0115	0.013	0.013
Co-60	1.0	$M_1 + M_2$	0.0400	0.0400	0.0400	0.040	0.040
Cs-137D	1.0	$M_1 + M_2$	0.0120	0.0120	0.0114	0.012	0.013
Co-60	5.0	$M_1 + M_2$	0.0020	0.0025	0.0025	0.0020	0.0020
Cs-137D	5.0	$M_1 + M_2$	0.0006	0.0006	0.0006	0.00062	0.00063

Cs-137D includes the progeny Ba-137m; Sr-90D includes the progeny Y-90.
M_1 — Cover material = thickness of 0.037 cm, density of 0.70 g/cm^3
$2M_1$ — Cover material = thickness of 0.074 cm, density of 0.70 g/cm^3

M_2 — Cover material = thickness of 0.040 cm, density of 1.1 g/cm^3

Using SkinDose for Estimations of Deep Dose Equivalent. In 10 CFR 20.1201, "Occupational dose limits for adults", reference is made to the deep dose equivalent (DDE). Paraphrasing from 10 CFR 20.1003, "Definitions", the DDE (H_d) applies to external whole-body exposure and is the dose equivalent at a tissue depth of 1 cm (1,000 mg/cm^2) averaged over the entire body. In various nuclear facilities and professions that use radioactive sources, there have been exposure instances in which small, sealed sources are placed in the pockets of clothing and result in potentially large radiation dose to the skin (and underlying organs). SkinDose can be used to calculate dose to a tissue depth of 1 cm, but that result should not be expressly applied to represent DDE (due to its definition).

In 2004, the Electric Power Research Institute (EPRI) released Report #1002823, "Implementing the EPRI Effective Dose Equivalent (EDE) Methodology for Discrete Radioactive Particles on the Skin" (EPRI 2004). The document provides a method of estimating DDE (using MCNP), but also states the following:

> "To calculate DDE at 1 cm depth tissue in this study, a cylindrical-shaped model consisting of tissue equivalent water with cross sectional area of 10 cm^2 and a height of 1.2 cm was used. The density of the tissue equivalent water is 1.0 g/cm^3, and the composition were based on those by Attix (1986). The isotropic point gamma source was simulated at 10 μm in air above the center of the tissue surface. The DDE is calculated as the dose at 1-cm below the tissue surface to a small disk having 2-mm radius and 70-μm thickness."

To mimic the EPRI estimation of DDE, the following inputs were used with SkinDose: (1) point geometry; (2) dose depth of 10 mm; (3) 1-hour exposure time; (4) 12.6 mm^2 averaging area; and (5) 10 μm airgap. Ignoring the 70-μm thickness at a depth of 1 cm will not influence the result. With these inputs, the SkinDose v2.0 results compared favorably with the EPRI results shown with three or four significant digits in Table 2-13 (refer to Table 3-11 of the EPRI document for details):

Table 2-13. Comparison of SkinDose v2.0 and EPRI (2004) estimates of deep dose

Energy (MeV)	SkinDose v2.0 (μSv h^{-1} MBq^{-1})	EPRI* (μSv h^{-1} MBq^{-1})
0.1	98	99.2
0.2	240	242
0.4	550	541
0.6	840	813
Cs-137D	790	764
0.662	930	-
0.8	1,100	1,098
1.0	1,300	1,319
1.25	1,600	-
Co-60	3,200	3,149
1.5	1,900	1,849
2.0	2,300	2,288

*using MCNP; Table 3-11 from EPRI (2004)

The comparison shows that SkinDose provides a photon dose estimate as valid as that provided by a probabilistic study using a rigorous Monte Carlo simulation for estimating a deep dose for discrete radioactive particles on the skin.

2.2.5. Limitations

The photon dosimetry model assumes that all volume sources are composed of air. This assumption results in greater accuracy when modeling larger, less dense sources (e.g., a gas cloud). However, when modeling volumetric sources of greater density, SkinDose is optimized for small dimensions (less than about a millimeter). This optimization is the result of a tradeoff between attenuation and charge particle buildup within the source itself. The user should exercise care when modeling large-volume sources (i.e., if the source is large enough to impact self-absorption of photons).

2.3. Alpha Dosimetry

Even at the shallow depth (7 mg/cm^2), the basal cells in tissue are usually protected from alpha particles on or above the skin because of its dead cellular layer (the stratum corneum). Alpha particles less than about 6.9 MeV will not penetrate this layer, and therefore will not contribute to the SDE. There are, however, a few radionuclides that emit alpha particles of considerable energy, enough to penetrate the dead layer and deposit energy at the shallow depth.

The alpha dose at a given depth is calculated from the mass stopping power of particles as they pass through the averaging area. The estimate of stopping power begins with the Bragg-Kleeman rule (Eq. [2.40]),

$$\Lambda_j^0 \rho_j \sqrt{M_{air}} = \Lambda_{air}^0 \rho_{air} \sqrt{M_j} \qquad [2.40]$$

to determine the linear range, Λ_j^0, of an alpha particle in material j given its range in air, Λ_{air}^0. As the equation indicates, this relationship is only a function of atomic mass (M) and density (ρ) of material j and air. The alpha dosimetry model is very sensitive to the tissue density parameter; therefore, a value of 1.1 g/cm^3 is used in the SkinDose alpha dosimetry model. This sensitivity is not as prevalent for electron and photon dosimetry. For the alpha dose calculations in SkinDose, the source is assumed to be a point on the top layer of material regardless of the selected geometry and covers of cotton and latex, an airgap, and tissue thickness are available for energy degradation before the alpha particle reaches the critical depth for SDE (Figure 2-23). Covers with thickness greater than 0.02 cm are assumed to be cotton, whereas those thinner than or equal to 0.02 cm are assumed to be latex. The order of material through which the alpha particle passes is not important and multiple covers may be specified. Table 2-14 gives the values of M_j and ρ_j for each of the absorbing materials (note that cotton and latex density as specified in Table 2-14 is used for alpha dosimetry and is not taken as the value(s) entered by the user for defining cover characteristics).

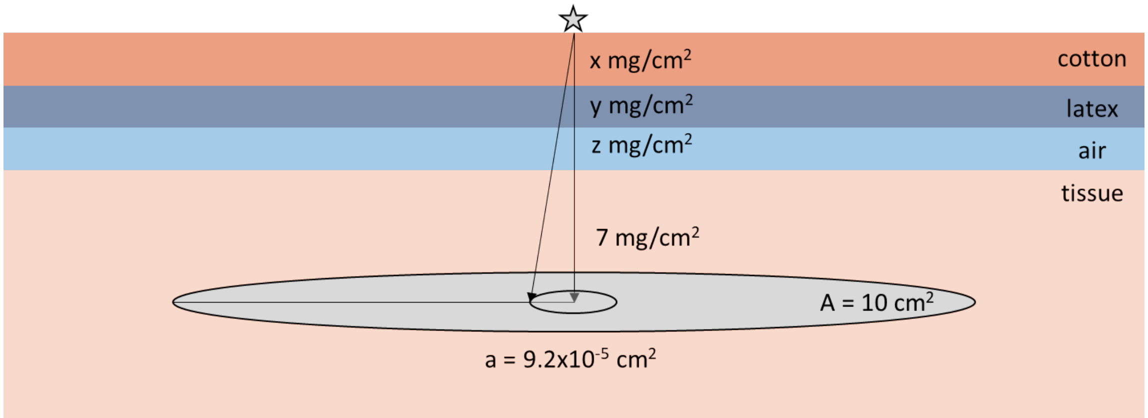

Figure 2-23. Diagram of Alpha Source Over the Skin Surface with Cover Materials of Cotton, Latex, and Air

Table 2-14. Material Constants

Material, j	**atomic mass, M_j (g/mol)**	**density, ρ_j (g/cm³)**
Air	14.661	0.0012
Cotton	13.294	1.55
Latex	12.591	0.97
Tissue	13.991	1.1

Starting with an initial alpha of energy E_0, its range through material j, Λ_j^0, is calculated with Eq. [2.41]:

$$\Lambda_j^0[cm] = \frac{\sqrt{M_j/M_{air}}}{\rho_j} EXP\left(\frac{a + b\sqrt{E_0} + cE_0}{1 + d\sqrt{E_0} + eE_0 + fE_0^{1.5}}\right), \quad [2.41]$$

where M_j is the atomic/molecular mass of material j, ρ_j is the bulk density of material j, alpha energy is in units of MeV, and the coefficients a through e are given in Table 2-15. The particle is assumed to travel through thickness l_j of material j, losing energy and possessing a residual range, $\Lambda_j^1 \rho_j$, after passage (Eq. [2.42]):

$$\Lambda_j^1 \rho_j \left[\frac{g}{cm^2}\right] = \left(\Lambda_j^0 - l_j\right) \rho_j. \quad [2.42]$$

At this point, the residual energy of the alpha particle is given by Eq. [2.43]:

$$E_1[MeV] = EXP\left(\frac{a + b\ln(\Lambda_j^1\rho_j) + c\ln(\Lambda_j^1\rho_j)^2 + d\ln(\Lambda_j^1\rho_j)^3}{1 + e\ln(\Lambda_j^1\rho_j) + f\ln(\Lambda_j^1\rho_j)^2 + g\ln(\Lambda_j^1\rho_j)^3 + h\ln(\Lambda_j^1\rho_j)^4}\right) \quad [2.43]$$

where coefficients a through h are defined in Table 2-15. The residual energy, E_1, is now the initial energy available for passing through the next cover layer. The process continues through each layer until the alpha energy is depleted or the dose depth in tissue is reached (e.g., typically 7 g/cm^2). At this depth and for the resulting residual energy, the mass stopping power, S/ρ, is calculated from Eq. [2.44]:

$$\frac{S}{\rho}\left[\frac{MeV\ cm^2}{g}\right] = \frac{a + bE_1 + cE_1{}^2 + dE_1{}^3}{1 + eE_1 + fE_1{}^2 + gE_1{}^3 + hE_1{}^4} \quad [2.44]$$

where energy is in units of MeV and the coefficients a through h are in Table 2-15.

Table 2-15. Coefficients for Equations

Coefficient	Eq. [2.41]	Eq. [2.43]	Eq. [2.44]
a	-14.553169	4.55197927	306.2468
b	-149.01176	1.742181919	15795.781
c	-6.1521278	0.229473336	15899.247
d	18.612154	0.010442972	8808.9471
e	2.279749	0.294283366	7.6456075
f	1.3839139	0.030560808	0.57467831
g		0.001341086	8.3211738
h		0.0000312944	1.1392825

The SDE to a receptor location i on an infinitely thin averaging disk is determined from, S_i/ρ, the mass stopping power at the receptor using Eq. [2.45]:

$$D_i = 1.6x10^{-7}\left[\frac{J\ g\ mSv}{MeV\ kg\ Sv}\right]\frac{S_i/\rho\left[MeV\ cm^2/g\right]\ w_R\left[Sv/Gy\right]\ Q[Bq]\ Y\left[\alpha/nt\right]\ t[h]}{4\ \pi\ l_i^2[cm^2]} \quad [2.45]$$

where w_R is the radiation weighting factor, Q is the source activity, Y is the alpha yield, and t is the time of exposure. The total travel length, l_i, from the point source to the point receptor i on the averaging disk (see Figure 2-23), is Eq. [2.46]

$$l_i = \sum_j l_j \qquad [2.46]$$

where $l_j = \frac{h_j}{\cos\theta_i}$ with similar relationships for the other three travel lengths, h_j is equal to the physical thickness of material j, and the angle, θ_i, in units of radians, is Eq. [2.47]

$$\theta_i = \tan^{-1}\left[\frac{r_{i-1} + \frac{(r_i - r_{i-1})}{2}}{h}\right] \qquad [2.47]$$

where r_i is the radius at point receptor i and h is the total physical thickness of covers, air, and tissue. Alpha dose is calculated at various receptor points along a single radius of the averaging disk (see Figure 2-23), along with an annular weight (Eq. [2.38]), to determine total dose (Eq. [2.48]) to the disk:

$$D = \sum_i D_i\, w_i. \qquad [2.48]$$

The method incorporated in SkinDose allows estimation of alpha dose equivalent to a given depth in tissue, while also considering the presence of cotton, latex, or air between the source and skin.

2.4. Cover Layer and Airgap Models

SkinDose is capable of modeling cover materials and airgaps. The models use the concept of effective path length to determine the electron energy lost in either a cover material or air before it enters the skin. The path length is not the true path traversed by the electron; rather, it is merely a mathematical convenience introduced to provide a measure of the energy lost in each layer. To minimize unintended applications of SkinDose, the airgap is limited to a maximum of 20 cm.

Figure 2-24 illustrates the method used to determine path length within the source and within the cover material. For the pictured cylindrical source, the known values in the figure are the source radius (R_{max}), the horizontal distance from the centerline to the source point (S_{RAD}), the source thickness (S_{THICK}), the cover thickness (C_{THICK}), the skin depth (S_{DEP}), the source and cover densities (ρ_s and ρ_c, respectively), the angular distance from the center of the dose area to the dose point (P_s), and the distance from the skin to the plane of the source point (D_{RAD}).

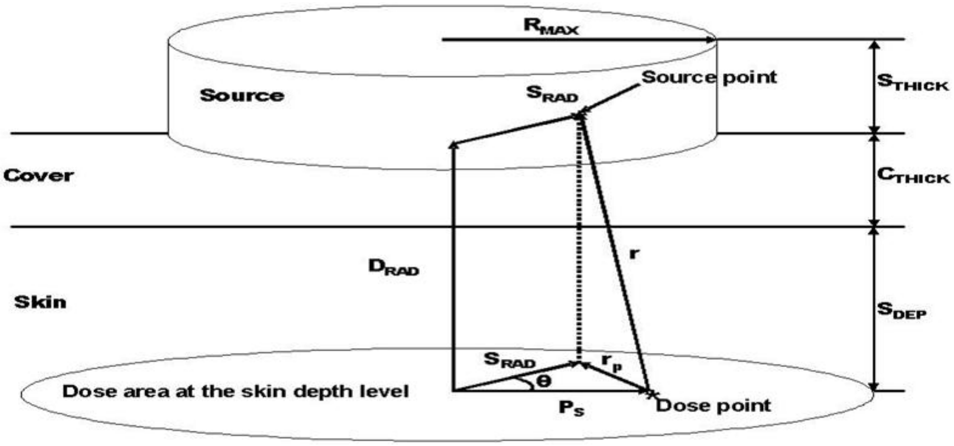

Figure 2-24. Schematic of a Generic Dose Calculation Performed by SkinDose for the Cylinder Geometry

The quadrature routines are coded to choose values for S_{RAD}, the distance from the centerline to the P_s source point; θ, the angle between S_{RAD} and P_s; and D_{RAD}, the height of the dose point. The first quantity to be calculated is r, the physical distance from a source point to a dose point. In this calculation, the square of the projected distance, r_p^2, is found using the law of cosines (Eq. [2.49]):

$$r_p^2 = P_s^2 + S_{rad}^2 - 2P_sS_{rad}cos\theta. \quad [2.49]$$

The quantity r is used in the denominator of the dose expression and represents the geometric attenuation between the dose point and the source point. This quantity is further analyzed to calculate the modified path length used to evaluate the scaled absorbed dose distribution.

By the law of similar triangles, the ratio to r of each of the actual distances along r through the source, the cover material, and the tissue is the same as the ratios of the thickness of the cover material to D_{RAD}, the thickness of tissue layer to D_{RAD}, and the remaining distance along r to D_{RAD} respectively, provided that the line connecting the dose point and the source point exits through the part of the source that is in contact with the cover material. Thus, the distance traveled through the cover material (Eq. [2.50]) is written as the following:

$$r_c = C_{thick} \cdot \left({}^{r}/_{D_{rad}} \right). \quad [2.50]$$

The distance traveled through the skin (Eq. [2.51]) is given by:

$$r_t = S_{dep} \cdot \left({}^{r}\!/_{D_{rad}} \right) \qquad [2.51]$$

and, the distance traveled through the source (Eq. [2.52]) is given by:

$$r_s = \left(D_{rad} - C_{thick} - S_{dep} \right) \cdot \left({}^{r}\!/_{D_{rad}} \right) \qquad [2.52]$$

For electron dosimetry, the modified path length r_1 is then found using Eq. [2.53]:

$$r_1 = \frac{(r_s\rho_s + r_c\rho_c + r_t\rho_t)}{\rho_t} \qquad [2.53]$$

where the variables ρ_s, ρ_c and ρ_t represent the density of the source, the cover material, and tissue, respectively. The density of tissue is assumed to be equal to that of water for the electron dosimetry model (1 g cm^{-3}).

For small-diameter sources, the path between the dose point and the source point may pass through the side of the source (e.g., the path may exit the source and traverse air before passing into skin). Thus, the quantity in Eq. [2.52] must be further analyzed to determine the path length within the source and the path length outside the source but above the level of the cover material. The actual path length within the source is multiplied by the source density, and the path length outside the source and above the cover material is multiplied by the density of the material outside the source, assumed to be air.

In spherical geometry, the physical distance from source point to dose point is given by Eq. [2.54]:

$$r_p^2 = P_s^2 + S_{rad}^2 sin^2\phi - 2P_sS_{rad}sin\phi cos\theta \qquad [2.54]$$

In slab geometry, the physical distance is given by Eq. [2.55]:

$$r = \sqrt{[(X_{source} - X_{dose})^2 + (Y_{source} - Y_{dose})^2 + (Z_{source} - Z_{dose})^2]} \qquad [2.55]$$

Anspach and Hamby (2018) and Dubeau et al. (2018) have shown that the cover and airgap models for electron dosimetry are too conservative (i.e., energy degradation of electrons appears to be too great as they travel through material before entering the skin). The user is cautioned not to rely on SkinDose for source geometries involving cover materials greater than a few centimeters.

2.5. Volume-Averaging Dose Model

The volume-averaging dose model allows the calculation of dose averaged over a given tissue volume. This model works with both photons and electrons yet is only truly meaningful for electron dose calculations. Any two planes of irradiated skin can be assigned to bound the skin volume. For sources in contact with the skin, the maximum penetration depth for electrons is equal to 1.8 times the X_{90} distance. Doses averaged over the dose-averaging area are calculated at 50 skin depths between two limits set by the user, and a cubic spline (a third-order piecewise polynomial curve fit) is fit to this depth-dose distribution. When the user specifies the skin depths corresponding to the volume of interest, SkinDose integrates the depth dose function over the region of interest to obtain the volume-averaged dose.

3.0 REFERENCES

Anspach, L.J. and D.M. Hamby, D.M. Performance of the VARSKIN 5 (v5.3) Electron Dosimetry Model. *Radiation Protection Dosimetry*. 181(2): 111-119. October 2018.

Attix, F.H. Introduction to Radiological Physics and Radiation Dosimetry. John Wiley & Sons. New York, NY. 1986.

Berger, M.J. "Distribution of Absorbed Dose around Point Sources of Electrons and Beta Particles in Water and Other Media." Medical Internal Radiation Dose Committee, Pamphlet No. 7. *Journal of Nuclear Medicine*. Vol. 12, Supplement No. 5. pp. 5–22. 1971.

Cross, W.G., N.O. Freedman, and P.Y. Wong. "Tables of Beta-Ray Dose Distributions in Water." AECL 10521, CA9200298. Chalk River Laboratories, Dosimetric Research Branch. Chalk River. Ontario, Canada. 1992.

Dubeau, J., S.S. Hakmana Witharana, J. Sun, B.E. Heinmiller, and W.J. Chase. A Comparison of Beta Skin Doses Calculated with VARSKIN 5.3 and MCNP5. *Radiation Protection Dosimetry*. DOI:10.1093/rpd/ncy108; July 2018.

Electric Power Research Institute (EPRI). Implementing the EPRI effective dose equivalent (EDE) methodology for discrete radioactive particles on the skin. Report No. 1002823. 2004.

International Commission on Radiological Protection (ICRP). "Radionuclide Transformations." Publication 38. Oxford, England: Pergamon Press. 1983.

International Commission on Radiation Protection (ICRP). "Nuclear Decay Data for Dosimetric Calculations." Publication 107. Ann. ICRP 38 (3). 2008.

International Commission on Radiation Units and Measurements (ICRU). "Tissue Substitutes in Radiation Dosimetry and Measurement." ICRU Report 44. Bethesda, MD: International Commission on Radiation Units and Measurements. 1989.

Johns, H.E. and J.R. Cunningham. The Physics of Radiology. 4th Edition. Springfield, IL: Charles C. Thomas. 1983.

Kawrakow, I. and D.W. Rogers. The EGSnrc code system: Monte Carlo simulation of electron and photon transport. *Technical Report* PIRS-701. Ottawa, Canada: National Research Council of Canada. 2000.

Ljungberg, M., S.E. Strand, and M.A. King. Monte Carlo Calculations in Nuclear Medicine, Second Edition. CRC Press. Chapter 10:175–195; 2012.

Los Alamos National Laboratory, X-5 Monte Carlo Team. “MCNP—A General Monte Carlo N-Particle Transport Code, Version 5. LA-CP-03-0245. Los Alamos, NM: LANL. 2003.

Mangini, C.D. “Beta-particle backscatter factors and energy-absorption scaling factors for use with dose-point kernels.” Doctoral Dissertation. *Oregon State University*. December 2012.

Mangini, C.D. and D.M. Hamby. “Scaling Parameters for Hot-Particle Beta Dosimetry”. *Radiation Protection Dosimetry*. 172(4): 356-366; 2016.

Sherbini, S., J. DeCicco, A.T. Gray, and R. Struckmeyer. “Verification of the Varskin Beta Skin Dose Calculation Computer Code,” *Health Physics.* 94: 527–538; 2008.

Spencer, L. V. Theory of Electron Penetration. *Physical Review.* 98: 1597-1615; 1955.

Spencer, L. V. Energy Dissipation by Fast Electrons. *National Bureau of Standards Monograph 1*; 1959.

U.S. Nuclear Regulatory Commission. Traub, R.J., W.D. Reece, R.I. Scherpelz, and L.A. Sigalla. “Dose Calculation for Contamination of the Skin Using the Computer Code VARSKIN.” NUREG/CR–4418. Washington, DC: NRC. 1987.

U.S. Nuclear Regulatory Commission. Reece, W.D., S.D. Miller, and J.S. Durham. “SADDE (Scaled Absorbed Dose Distribution Evaluator), A Code to Generate Input for VARSKIN.” NUREG/CR–5276. Washington, DC: NRC. 1989.

U.S. Nuclear Regulatory Commission. Durham, J.S. “VARSKIN Mod 2 and SADDE Mod 2: Computer Codes for Assessing Skin Dose from Skin Contamination.” NUREG/CR-5873, PNL-7913. Washington, DC: NRC. 1992.

U.S. Nuclear Regulatory Commission. Durham, J.S. “VARSKIN 3: A Computer Code for Assessing Skin Dose from Skin Contamination.” NUREG/CR-6918. Washington, DC: U.S. Nuclear Regulatory Commission. 2006.

U.S. Nuclear Regulatory Commission. Hamby, D.M., Lodwick, C.J., Palmer, T.S., Reese, S.R., Higley, K.A. “VARSKIN 4: A Computer Code for Skin Contamination Dosimetry.” NUREG/CR-6918, Rev 1. Washington, DC: U.S. Nuclear Regulatory Commission. 2011.

U.S. Nuclear Regulatory Commission. Hamby, D.M., Mangini, C.D., Caffrey, J.A., Tang, M. “VARSKIN 5: A Computer Code for Skin Contamination Dosimetry.” NUREG/CR-6918, Rev 2. Washington, DC: U.S. Nuclear Regulatory Commission. 2014.

U.S. Nuclear Regulatory Commission. Hamby, D.M., Mangini, C.D. “VARSKIN 6: A Computer Code for Skin Contamination Dosimetry.” NUREG/CR-6918, Rev 3. Washington, DC: U.S. Nuclear Regulatory Commission. 2018.

U.S. Nuclear Regulatory Commission. Hamby, D.M., Mangini, C.D.; Luitjens, J.; Boozer, D.L.; Tucker, Z.G.; Rose, C.T.; Flora, R.S. “VARSKIN+ 1.0: A Computer Code for Skin Contamination and Dosimetry Assessments.” NUREG/CR-6918, Rev 4. Washington, DC: U.S. Nuclear Regulatory Commission. 2021.